2016-06-17

The relationship between eruptive activity, flank collapse, and sea level at volcanic islands: A long-term (>1 Ma) record offshore Montserrat, Lesser Antilles

Coussens, M

http://hdl.handle.net/10026.1/4930

1 **The relationship between eruptive activity, flank collapse and sea-level at volcanic**

2 **islands: a long-term (>1 Ma) record offshore Montserrat, Lesser Antilles**

3

4 **Maya Coussens**

5 *School of Ocean and Earth Science, National Oceanography Centre, University of*

6 *Southampton, European Way, Southampton, SO14 3ZH, UK (mfc1e12@soton.ac.uk)*

7

8 **Deborah Wall-Palmer**

9 *School of Geography, Earth and Environmental Sciences, Plymouth University, Plymouth*

10 *PL4 8AA, UK (deborah.wall-palmer@plymouth.ac.uk)*

11

12 **Peter. J. Talling**

13 *National Oceanography Centre, Southampton, Southampton S014 3ZH, UK*

14 *(peter.talling@noc.ac.uk)*

15

16 **Sebastian. F. L. Watt**

17 *School of Geography, Earth and Environmental Sciences, University of Birmingham,*

18 *Edgbaston, Birmingham, B15 2TT, UK (s.watt@bham.ac.uk)*

19

20 **Michael Cassidy**

21 *Institute of Geosciences, Johannes Gutenberg, University Mainz, J- J- Becher- Weg 21,*

22 *D-55128, Mainz, Germany (mcassidy@uni-mainz.de)*

23

24 **Martin Jutzeler**

25   *National Oceanography Centre, Southampton, University of Southampton, Southampton*

26   *S014 3ZH, UK (jutzeler@gmail.com)*

27

28   **Michael. A. Clare[1], James. E. Hunt[2]**

29   *National Oceanography Centre, Southampton, Southampton S014 3ZH, UK*

30   *(michael.clare@noc.ac.uk)[1], (James.Hunt@noc.ac.uk)[2]*

31

32   **Michael Manga**

33   *Department of Earth & Planetary, Science University of California, Berkeley, 307*

34   *McCone Hall, Berkeley, CA, 94720, USA (manga@seismo.berkeley.edu)*

35

36   **Thomas. M. Gernon[1], Martin. R. Palmer[2], Stuart. J. Hatter[3]**

37   *School of Ocean and Earth Science, National Oceanography Centre, University of*

38   *Southampton, European Way, Southampton, SO14 3ZH, UK*

39   *(Thomas.Gernon@noc.soton.ac.uk)[1], (m.palmer@noc.soton.ac.uk)[2],*

40   *(sjh1e13@soton.ac.uk)[3]*

41

42   **Georges Boudon**

43   *Équipe de Géologie des Systèmes Volcaniques, Institut de Physique du Globe de Paris,*

44   *Sorbonne, Paris Cité, UMR 7154 CNRS, 1 Rue Jussieu Paris, 75238, France*

45   *(boudon@ipgp.fr)*

46

47   **Daisuke Endo**

48   *Earth Evolution Sciences, University of Tsukuba, Tennodai 1-1-1, Tsukuba, Ibaraki, 305-*

49   *8572, Japan (daisuke.endo.000@gmail.com)*

50

51 **Akihiko Fujinawa**

52 *Research Institute for Natural Hazards and Disaster Recovery, Niigata University,*

53 *Ikarashi 2-8050, Nishi-ku, Niigata, 950-2181, Japan*

54 *(fujinawa.INET.TheWorld@iodp.tamu.edu)*

55

56 **Robert Hatfield**

57 *9 College of Oceanic and Atmospheric Sciences, Oregon State University, 104 COAS*

58 *Administration Building, Corvalis, OR 97331-5503, USA*

59 *(rhatfield@coas.oregonstate.edu)*

60

61 **Matthew. J. Hornbach**

62 *Institute for Geophysics, University of Texas at Austin, J.J. Pickle Research Campus,*

63 *Building 196, 10100, Burnet Road, Austin, TX, 78758-4445, USA*

64 *(matt.hornbach@gmail.com)*

65

66 **Osamu Ishizuka**

67 *Geological Survey of Japan (AIST), Central 7, Higashi 1-1-1, Tsukuba, Ibaraki, 305-8567,*

68 *Japan (o-ishizuka@aist.go.jp)*

69

70 **Kyoko Kataoka**

71 *Research Institute for Natural Hazards and Disaster Recovery, Niigata University,*

72 *Ikarashi 2-8050, Nishi-ku, Niigata, 950-2181, Japan (kataoka@gs.niigata-u.ac.jp)*

73

74 **Anne Le Friant**

75 *Équipe de Géologie des Systèmes Volcaniques, Institut de Physique du Globe de Paris,*

76 *Sorbonne, Paris Cité, UMR 7154 CNRS, 1 Rue Jussieu Paris, 75238, France*

77 *(lefriant@ipgp.fr)*

78

79 **Fukashi Maeno**

80 *Earthquake Research Institute, University of Tokyo, 1-1-1 Yayoi, Bunkyo-ku, Tokyo, 113-*

81 *0032, Japan (fmaeno@eri.u-tokyo.ac.jp)*

82

83 **Molly McCanta**

84 *Department of Geology, Tufts University, 2 North Hill Road, Lane Hall Medford, MA*

85 *02155, USA (molly.mccanta@tufts.edu)*

86

87 **Adam. J. Stinton**

88 *Montserrat Volcano Observatory, Flemmings, Montserrat (adam@mvo.ms)*

89

90 *Seismic Research Center, University of the West Indies, St. Augustine, Trinidad and*

91 *Tobago*

92

93 **Key Points**

94 Heightened volcanic activity on Montserrat at 120-190 ka, 760-810 ka, and 900-930 ka

95 Large landslides coincide with rapid sea-level rise at island arc volcanoes

96

97   **Abstract**

98

99   Hole U1395B, drilled southeast of Montserrat during Integrated Ocean Drilling Program

100   Expedition 340, provides a long (>1 Ma) and detailed record of eruptive and mass-

101   wasting events (>130 discrete events). This record can be used to explore the temporal

102   evolution in volcanic activity and landslides at an arc volcano. Analysis of tephra fall and

103   volcaniclastic turbidite deposits in the drill cores reveals three heightened periods of

104   volcanic activity on the island of Montserrat (~930 ka to ~900 ka, ~810 ka to ~760 ka,

105   and ~190 ka to ~120 ka) that coincide with periods of increased volcano instability and

106   mass-wasting. The youngest of these periods marks the peak in activity at the Soufrière

107   Hills volcano. The largest flank collapse of this volcano (~130 ka) occurred towards the

108   end of this period, and two younger landslides also occurred during a period of relatively

109   elevated volcanism. These three landslides represent the only large (>0.3 km^3) flank

110   collapses of the Soufrière Hills edifice, and their timing also coincides with periods of

111   rapid sea-level rise (>5 m/ka). Available age data from other island arc volcanoes

112   suggests a general correlation between the timing of large landslides and periods of rapid

113   sea-level rise, but this is not observed for volcanoes in intra-plate ocean settings. We thus

114   infer that rapid sea-level rise may modulate the timing of collapse at island arc volcanoes,

115   but not in larger ocean-island settings.

116

117   **Key words**

118   Landslide, volcanism, sea-level, IODP, Expedition 340

119

120   **1. Introduction**

121

122   Volcanic islands in arc settings grow and decay through eruptive and mass-wasting

123   processes. The rate of island growth reflects the balance of these processes, including the

5

124   style, composition and magnitude of individual eruptions [Houghton et al., 1995; Singer

125   et al., 2008; Germa et al., 2010], and variations in the magnitude and frequency of mass-

126   wasting events (e.g. lava dome collapses, flank landslides) [Ablay and Marti, 2000; Cole

127   et al., 2002; Trofimovs et al., 2013]. As a volcanic island grows, the edifice becomes

128   increasingly unstable, resulting in partial flank collapses, which are a ubiquitous feature

129   of composite volcanoes (e.g. Siebert, 1984). Such collapse events are potential geohazards

130   through the generation of landslides [Siebert, 1984; Watt, et al., 2012a, 2012b], and their

131   potential to generate tsunamis [Ward and Day, 2003]. There are few individual volcanic

132   records that span the life cycle of individual composite volcanoes (on the order of 10^5 to

133   10^6 years), but such records can be used to investigate temporal patterns in total volcanic

134   output, and the relative timing of flank collapses. The instabilities that drive collapses

135   may relate both to internal (e.g. total volcanic output) and external (e.g. eustatic sea-level

136   change) processes. To obtain a more complete understanding of the overall controls on

137   volcano growth and destruction, we use a marine stratigraphic record offshore Montserrat

138   to explore patterns of volcanism, sea-level change and flank collapse timing over a 10^6

139   year period.

140

141   Here, we use the term flank collapse to refer to gravity-driven failures of volcanic

142   material from subaerial and/or submarine volcanic island flanks, potentially also

143   involving carbonate shelf material. Collapses that only involve material from the

144   carbonate shelf (i.e. generating bioclastic deposits) are referred to as shelf collapses. Flank

145   collapses can involve several cubic kilometres of material, and may or may not be

146   associated with volcanic eruptions. They are distinct from the generally smaller dome

147   collapses, which involve juvenile lava and are a common mass wasting process during the

148   lava-dome forming eruptions that typify volcanism on Montserrat. *Mass-wasting* or

149   *landslides* are used as collective terms here for the different types of collapse events.

150   Landslides may also generate a range of density currents that are represented in the

151   geological record as a variety of density current deposits. In this study we refer to all

152   submarine density current deposits as *turbidites*, regardless of whether the deposits were

153   generated from fully turbulent or non-turbulent flows.

154

155   Triggers of flank or shelf collapses on volcanic islands are poorly understood, but it has

156   been proposed that their frequency is related to eustatic sea-level changes, edifice growth,

157   tectonic activity, and rainfall [McGuire et al., 1997; Masson et al., 2006; Sato et al., 2007;

158   Marques et al., 2008; Quidelleur et al., 2008; Hunt et al., 2013, 2014]. Reconstructing pre-

159   historical earthquake and rainfall records are challenging, resulting in difficulties when

160   comparing these potential triggers to landslide occurrence. Previous studies of eustatic

161   sea-level change and landslides have been hampered due to difficulties in acquiring

162   sufficient and accurate dates for landslide events. Such studies have typically relied on

163   incomplete information from on-land observations of collapse structures, and/or been

164   restricted to relatively recent events recorded in shallow (<6 m) marine sediment cores

165   and seismic profiles [McMurtry et al., 2004a, 2004b; Boudon et al., 2007; Trofimovs et

166   al., 2013]. Consequently, very few volcanic island landslide events have been dated

167   precisely over time periods that are long enough to include multiple climatic, volcanic,

168   and tectonic cycles [Longpré et al., 2011; Trofimovs et al., 2013; Hunt et al., 2013].

169

170   We analysed Hole U1395B from IODP Expedition 340, drilled in 2012. This Hole is

171   >120 m in length and contains an unusually long (>1 Ma) and detailed marine record of

172   island arc volcanism and mass-wasting activity. Hole U1395B was drilled ~25 km

173   southeast of Montserrat at ~1200 m below sea-level (Figure 1), and provides an excellent

174   opportunity to study a long and detailed record of sedimentological processes around an

175   island arc volcano.

176

177   The record of marine volcaniclastic deposits (both turbidites and tephra fall deposits) is

178   used as a proxy for volcanic activity at Montserrat. This approach is based on studies of

179   marine deposits associated with the 1995-2010 eruption on Montserrat [Kokelaar, 2002;

180   Trofimovs et al., 2006], which showed that individual pyroclastic flows formed via dome-

181   collapse and explosive eruption events produced widespread volcaniclastic turbidites. We

182   thus expect most volcaniclastic turbidites to represent individual eruptions, but note that

183   some volcaniclastic turbidites may be produced by non-eruptive flank collapses, or by

184   reworking of older volcaniclastic deposits. Turbidites from large flank collapses can be

185   identified by their thickness and correlation with debris avalanche deposits (and there are

186   only a few of these around Montserrat; cf. Lebas et al., 2011), while resedimented

187   turbidites may be more mixed, including bioclastic material. The latter may also still

188   provide a broad proxy for volcanic activity, since they are more likely to be generated

189   during periods of volcanism, when flanks may be destabilised by eruptive activity and

190   deposition of volcanic products [Collins and Dune et al., 1986; Major et al., 2000; Hunt et

191   al., 2014].

192

193   By identifying and dating volcaniclastic deposits from Hole U1395B, we aim to

194   investigate the temporal relationships between mass-wasting, volcanic activity, and sea-

195   level over an interval of ~10^6 years. This period encompasses a sufficient number of

196   volcanic cycles and eustatic sea-level changes to allow for statistically robust hypothesis

197   testing. It is also shown that all of the well-dated major collapse events around Montserrat

198   occurred during periods of rapid sea-level rise. We explore whether other volcanic islands

199 (island arcs and intraplate ocean islands) show similar relationships between landslide

200 ages and sea level or volcanism, whilst noting that many of these landslide ages have

201 considerable uncertainties.

202

203

204 **2. Study Area: Introduction to Montserrat**

205

206 Montserrat is an island arc volcano located in the Lesser Antilles (Figure 1), which

207 erupted between 1995-2010, devastating the city of Plymouth and affecting large parts of

208 the island economy [Kokelaar et al., 2002; Wadge et al., 2014]. The eruptions included

209 collapse of the active lava dome generating pyroclastic flows and block and ash flows.

210 The largest dome collapse (0.21 km^3) occurred in 2003 and generated a 0.5-1 m high

211 tsunami on Guadeloupe [Herd et al., 2006; Trofimovs et al., 2008]. Bathymetric mapping

212 has since identified much larger landslide deposits offshore Montserrat with volumes of

213 0.3-20 km^3 [Deplus et al., 2001; Boudon et al., 2007; Lebas et al., 2011; Watt et al., 2012a,

214 2012b]. Such large landslides have a much higher tsunamigenic potential, and thus

215 represent a more significant hazard than events associated with the recent eruptions.

216

217 Since ~290 ka (based on subaerial Ar-Ar dates; Harford et al., [2002]), activity at

218 Montserrat has been focussed on the andesitic Soufrière Hills volcano, except for a brief

219 interlude of basaltic volcanism at ~130 ka, forming the South Soufrière Hills (Figure 1).

220 The previously active volcanic centre, at Centre Hills, is dated at 990-550 ka [Harford et

221 al., 2002]. Between these two periods of activity (550 ka to 290 ka) the subaerial record

222 suggests a period of quiescence. The apparent gap in volcanism from 550 ka to 290 ka is

223 not clear in the marine sediment cores, and the existing subaerial ages may thus reflect a

224   limited stratigraphy represented by on-land exposures, or incomplete study and dating of

225   subaerial outcrops.

226

227   The offshore eruption and landslide record around Montserrat has been studied in detail

228   [Deplus et al., 2001; Trofimovs et al., 2006, 2010, 2012, 2013; Boudon et al., 2007; Lebas

229   et al., 2011; Le Friant et al., 2010, 2015; Cassidy et al., 2012b, 2013]. To the southeast

230   and southwest of Montserrat is an extensive shallow core (<6 m) data set (Figure 1).

231   These >80 cores contain hemipelagic sediment and numerous volcaniclastic and bioclastic

232   turbidites from eruption and landslide deposits emplaced during the last ~110 ka [Le

233   Friant et al., 2009; Trofimovs et al., 2010, 2012, 2013; Cassidy et al., 2012b, 2013].

234   Swath bathymetry and 2D and 3D seismic data reveal seven large landslide deposits,

235   dating back to the time of Centre Hills volcanism (Figure 1). These large landslide

236   deposits likely represent flank collapse events as opposed to dome or localised shelf

237   collapses.

238

239   It is important to recognise that any study based on a single sampling site will introduce

240   some sampling bias in the record of eruptive and collapse events. The activity at

241   Montserrat is typified by dome-forming eruptions with durations of months to years,

242   interspersed by moderate-sized explosive pulses such as the 1995-2010 eruption

243   [Kokelaar, 2002; Wadge et al., 2014]. Such eruptions form complex volcaniclastic

244   intervals generated by multiple pyroclastic density currents and tephra fall events

245   distributed radially from the volcanic edifice [Trofimovs et al., 2006, 2013; Le Friant et

246   al., 2015]. Hole U1395B is located ~25 km southeast of Montserrat, hence it is only likely

247   to sample mass flows that entered the ocean to the east and south of Montserrat. While

248   some individual events may therefore not be preserved within Hole U1395B, periods of

249   eruption are still likely to be represented, because any one eruption is likely to produce

250   multiple mass flow and tephra fall deposits, with the mass flows, in particular, travelling

251   in a range of directions. For example, the 2003 collapse event (0.1 km^3) deposited a ~20

252   cm thick volcaniclastic turbidite at site U1395B [Trofimovs et al., 2008], but small

253   vulcanian eruptions that occurred throughout the 1995-2010 eruption are not represented

254   within Hole U1395B [Kokelaar, 2002; Wadge et al., 2014].

255

256   Hole U1395B is only likely to sample a small proportion of tephra fall deposits, as

257   dispersal depends on wind direction and the magnitude of the explosive event. Prevailing

258   wind directions in the troposphere and upper stratosphere are predominantly from the east,

259   and prevailing wind directions in the lower stratosphere are from the west, based on

260   historical data from 1956 to present [Radiosonde wind dataset on Guadeloupe]. Tephra

261   fall deposits may therefore be subject to a spatial sampling bias, with many eruption

262   plumes transported to the west leaving no record within U1395B. However, large

263   explosive eruptions, which can involve multiple phases and be associated with pyroclastic

264   density currents and the generation of offshore turbidites, are still likely to have some

265   representation at the core site as an eruptive event. Because we are interested simply in

266   event timing, rather than magnitude or style, this single core is likely to provide a

267   relatively comprehensive record of eruptions at Montserrat.

268

269

270   **3. Methods**

271

272   *3.1. Event deposit identification*

273   We defined five facies at Site U1395: hemipelagic mud, bioclastic turbidites, mixed

274   bioclastic-volcaniclastic turbidites, volcaniclastic turbidites, and tephra fall deposits

275   (Figure 2). Hemipelagic mud is mostly composed of carbonate and detrital clay with

276   abundant interspersed foraminifera. The volcaniclastic turbidite and tephra fall deposits

277   are less easily distinguished from each other, as both can comprise normally-graded sand

278   and silt [Trofimovs et al., 2013]. Their discrimination requires grain size and component

279   analysis to identify the type of event deposit [Cassidy et al., 2014, 2015].

280

281   Tephra fall layers were defined in this study as having <30% bioclasts, a Folk and Ward

282   [1957] sorting coefficient of <0.5 phi (where grainsize (phi) = - $\log_2$(grainsize (mm))

283   (analyses conducted on particles from -1 to 9 phi), and a thickness of <20 cm. Tephra fall

284   deposits are well sorted by density and dominated by volcanic clasts. Hole U1395B is ~25

285   km away from Montserrat, where tephra fall deposits from moderate-sized explosive

286   eruptions, even downwind, are likely to be a few centimetres thick; consequently, thick

287   (>20 cm) deposits are unlikely to represent tephra fall layers. Large magnitude eruptions

288   are rare within the Lesser Antilles [Palmer et al., 2016]. Thin tephra fall layers are

289   commonly mixed with surrounding hemipelagic material, through bioturbation, bottom

290   current reworking, or disturbance during coring, thus artificially increasing their apparent

291   bioclast content. We thus examined the core for any evidence of post-depositional

292   processes (Supplementary figure S1) and have defined tephra fall layers as comprising <

293   30% bioclast content to allow for post-depositional mixing. Volcaniclastic turbidites are

294   deposits from high-energy, erosive flows that may entrain bioclastic material and pre-

295   existing volcaniclastic sediments. Therefore, although some parts of a volcaniclastic

296   turbidite can be well-sorted, they are likely to be less well-sorted than tephra fall deposits

297   [Cassidy et al., 2014]. Volcaniclastic turbidites are defined here as comprising <30%

298   bioclasts, with a Folk and Ward [1957] sorting coefficient >0.5 (phi). Mixed turbidites are

299   defined as having 30-70% bioclasts. Bioclastic turbidites are defined as containing >70%

300   bioclasts (see Supplementary Figures S1-S3).

301

302   Grain size measurements using laser-diffraction analyses were carried out using a

303   Malvern Master-sizer 2000 particle size analyser, which can measure grain sizes between

304   0.2−2000 μm. To disperse grains, 25 ml of reverse osmosis water with 0.05% sodium

305   hexametaphosphate dispersant was added to 1 cm^3 of sample and left overnight on a

306   shaking table. Samples were analysed in triplicate and accuracy was monitored using

307   standard size particles (32 and 125 μm) (see Hunt et al., [2013] for details). Componentry

308   analysis was conducted on sieved fractions >63 μm and <250 μm material from all

309   volcanic-rich units and some bioclastic-rich units. For each sample, approximately 400

310   grains were point-counted using an area counting method. Componentry classes follow Le

311   Friant et al., [2008] and Cassidy et al., [2014]: 1) vesicular pumice clasts; 2) non-vesicular

312   andesite; 3) altered lithic clasts; 4) crystal and glass fragments; 5) mafic scoria clasts; and

313   6) bioclasts. Grainsize and componentry data are summarized in Table S1 and Table S2,

314   respectively (see Supplementary Figures S1-S3 for photos).

315

316   *3.2. Dating Hole U1395B*

317   The core from U1395B core was dated using a combination of oxygen isotope

318   stratigraphy, biostratigraphy, AMS radiocarbon dating, and the shipboard paleomagnetic

319   reversal records. Higher resolution dating was carried out on the upper 40 m of Hole

320   U1395B using oxygen isotope stratigraphy of the hemipelagic mud (Figure 2). Twenty

321   *Globigerinoides ruber* specimens between 250-355 μm in size were picked and analysed

322   from each hemipelagic sample. Samples were 7 cm apart and analysed at Plymouth

323   University on an Isoprime Instruments continuous flow mass spectrometer with a Gilson

324   Multiflow carbonate auto-sampler. Oxygen Isotope values are given as deviations in the

325   isotope ratios ($^{18}O/^{16}O$) per mil (‰), using the VPDB scale (Table S3).

326

327   To limit the ambiguity of identifying marine isotope stages, biostratigraphic boundaries

328   and AMS radiocarbon dates (for sediments <50 ka) were used (Table 1).

329   Calcareous nannofossils in the <63 μm material from hemipelagic samples were analysed

330   using scanning electron microscopy (SEM), employing the calcareous nannofossil

331   zonation of Kameo and Bralower [2000] for the Caribbean Sea. Sediment was fixed to

332   metal stubs using a thin layer of spray adhesive, then sputter-coated with gold. The first

333   occurrence of *Emiliania huxleyi* (250 ka) was found at 36.74 m, close to the MIS 7/8

334   boundary (243 ka). The first occurrence of *E. huxleyi* has also been identified across the

335   MIS 7/8 transition in Hole U1396C [Wall-Palmer et al., 2014] and CAR-MON 2 [Le

336   Friant et al., 2008] (Figure 3).

337

338   New AMS dates were obtained in this study from four samples in the upper 4 m of Hole

339   U1395B (aged <57 ka), in addition to the radiocarbon AMS dates reported by Trofimovs

340   et al., [2013]. Approximately 1000 pristine tests of white *Globgerinoides ruber* >150 μm

341   in size were picked (~17 mg) and then sonically cleaned. The new samples were located

342   beneath two of the largest turbidites (Figure 3). Radiocarbon dates were measured at

343   Scottish Universities Environmental Research Council (SUERC) using their in-house

344   protocol [see Trofimovs et al., 2013].

345

346   Paleomagnetic reversals were determined on board during Expedition 340 as 180°

347   changes in declination (after azimuthal correction). Associated changes in inclination after

14

348   demagnetization of the natural remnant magnetization (NRM) in a field of 20 mT (to

349   remove the coring overprint) were also recorded (see Hatfield et al., [2013] for details).

350   Here we report ages based on the geomagnetic polarity timescale (GPTS) of Ogg et al.,

351   [2012] instead of the GPTS of Cande and Kent [1995] as was reported on board the ship.

352   Two paleomagnetic reversals occur at 781 ka (6.3% error) and 988 ka (11.3% error) in

353   core U1395B [Cande and Kent 1992a, 1992b; Ogg et al., 2012], with a possible third

354   reversal at the base of the core at 1072 ka (11.3% error) [Cande and Kent 1992; Ogg et al.,

355   2012]. The 781 ka reversal is obscured by a volcaniclastic turbidite and coring

356   disturbance at 68.5-71 m (Figure 2). The coring disturbance occurs primarily within the

357   volcaniclastic turbidite. The reversal is likely to have occurred shortly prior to the

358   emplacement of the volcaniclastic turbidite, thus obscuring the reversal through erosion of

359   hemipleagic mud. Here we take the base of the volcaniclastic turbidite as 781 ka. The

360   MIS 8/9 (300 ka) boundary is interpreted to occur at ~44 m, suggesting that sedimentation

361   rates decrease with depth in the core. The 988 ka reversal occurred between 88.3-89.9m

362   with a mid-point at 89.1 m (Figure 2). The 1072 ka reversal may be present at the base of

363   Hole U1395B (Figure 2) but this is less certain due to poor sample recovery at the base of

364   the core.

365

366   Data from Hole U1395B were also compared and correlated to previously studied cores

367   around Montserrat (Figure 3). These cores include JR123-5V, JR123- 6V, CAR-MON 2,

368   and Hole U1396C (Figure 3). JR123-5V and JR123-6V are part of an extensive vibrocore

369   data set that has been used to compile a comprehensive stratigraphy of Montserrat over

370   the past 110 ka [Trofimovs et al., 2013]. The vibrocore data set includes over 80 <6 m

371   long cores with 40 accelerator mass spectrometry (AMS) radiocarbon dates (Figure 3).

372   JR123-5V and JR123-6V are located 1-2 km north of Site U1395, and some units within

373 core U1395B can be correlated to units found in JR123-5V and JR123-6V by age (Figure

374 3). CAR-MON 2 is a piston core collected in 2002, which extends 5.75 m and was taken

375 ~55 km to the southwest of Montserrat (Figure 3) [Le Friant et al., 2008]. Site U1396C is

376 situated ~33 km southwest of Montserrat (Figure 3) and was collected during IODP

377 Expedition 340 [Wall-Palmer et al., 2014].

378

379

380 **4. Results**

381

382 Hole U1395B is 127.51 m long and it is composed of 62.6% hemipelagic mud, 24.4%

383 volcaniclastic deposits, 9% mixed turbidites and 4% bioclastic deposits, by deposit

384 thickness. The core comprises 18 bioclastic turbidites, 48 tephra fall deposits, 26 mixed

385 turbidites, and 41 volcaniclastic turbidites. Core recovery is good (>90%), with only one

386 occurrence of basal flow-in coring disturbance over the studied core length at the bottom

387 of Core U1395B-2H, followed by probable fall-in at the top of Core Section U1395B-3H

388 [Jutzeler et al., 2014].

389

390 *4.1. Age Models*

391 Unit ages have been estimated by calculating hemipelagic sedimentation rates between

392 dated horizons, assuming constant sedimentation rates between dated horizons.

393 Devoloping accurate age models for marine cores is difficult due to the effects of erosion

394 (commonly at the base of turbidites), short-term fluctuations in sediment supply, and the

395 sometimes ambiguous identification of marine isotope stages. We therefore include three

396 age models to help capture these uncertainties, and their implications.

397

398   Age models can be affected by erosion. In the upper 5 m of U1395B ~88 cm of

399   hemipelagic sediment may have been eroded by the 12-14 ka turbidite [Trofimovs et al.,

400   2013], indicating that the effects of erosion at Site U1395B may be significant. Erosion

401   rates in the upper 10 m of U1395B are well constrained by a combination of AMS dates

402   from this study, and correlation with well-dated units (40 AMS dates) in the shallow

403   vibrocore dataset [Trofimovs et al., 2013]. Below the threshold for AMS radiocarbon

404   dating (>10 m in Hole U1395B) the effects of erosion by turbidites cannot be accurately

405   constrained at site U1395B, potentially leading to inaccuracies in age models. It is likely

406   that most turbidity currents are erosive, removing underlying hemipelagic mud and event

407   deposits from the stratigraphy resulting in the underestimation of the true sedimentation

408   rate. We expect this to be a systematic error affecting the whole core, however, rather

409   than something that introduces bias to specific time periods.

410

411   Dating cores using oxygen isotopes may also lead to age model inaccuracies due to

412   difficulties in identifying marine isotope stages (MIS). Oxygen isotopes from Hole

413   U1395B have been compared to the Lisiecki and Raymo, [2005] curve; but, local factors

414   may affect the magnitude of isotope fluctuations and erosion may remove parts of the

415   isotope record, resulting in the misidentification of MIS boundaries. Any inaccuracies in

416   the age models used will affect the reliability of unit ages assigned to individual events,

417   and thus affect subsequent analysis of the dataset.

418

419   Assuming that the average total erosion beneath turbidites is on the order of centimetres,

420   and assuming that MIS boundaries have been correctly constrained within a few

421   centimetres, the event dating errors are likely to be on the order of 10^2-10^5 years. This is

422   of a similar magnitude to stratigraphic gaps identified in other cores around Montserrat,

423   including instances where >30 ka of stratigraphy was removed by turbidite erosion (JR

424   123-5-V and Hole U1396C) (Trofimovs et al., 2013; Wall-Palmer et al., 2014). In order to

425   assess how sensitive our event-frequency analysis is to dating errors of this magnitude, we

426   conduct the same analysis with three different age models. Age Model 1, described below,

427   uses all age constraints (i.e. MIS boundaries, palaeomagnetic reversals etc.) but is also

428   potentially more susceptible to the effects of erosion, producing a record with apparent

429   fluctuations in sedimentation rate. Age Models 2 and 3 use fewer age constraints,

430   resulting in a smoother estimate of long-term sedimentation rate that may be more

431   geologically realistic. Individual unit ages derived from the three age models may vary by

432   up to 10^5 years. By using all three age models within subsequent analyses, we can test

433   how robust our results are to these uncertainties.

434

435   **Age Model 1:** This model uses 11 dated horizons, including horizons derived from

436   correlations to units described in Trofimovs et al. [2013], identification of MIS

437   boundaries, and identification of paleomagnetic reversals. The 2-1.5 ka, 6 ka, 14 ka, 74-59

438   ka, 110-103 ka, and 130 ka deposits from Trofimovs et al. [2013] and Cassidy et al.

439   [2013] have been correlated to units in U1395B. Unit ages of 1.75 ka, 6 ka, 14 ka, 66.5 ka,

440   107 ka, and 130 ka in Hole U1395B at core depths of 0.49 m, 2.52 m, 3.98 m, 6.26 m,

441   10.47 m, and 18.49 m respectively were used in age model 1. Using oxygen isotope

442   analysis 3 MIS boundaries were identified and used. These are MIS boundaries 6/7 (191

443   ka), 7/8 (243 ka) and 8/9 (300 ka) at core depths of 28.31 m, 35.93 m, and 43.84 m

444   respectively [Lisiecki and Raymo. 2005]. Finally, two paleomagnetic reversal dates of

445   781 ka, and 988 ka, at depths of 63.06 m, and 89.08 m are used in age model 1.

446

447   Using Age Model 1, the calculated sedimentation rates in the upper 300 ka of Hole

448   U1395B fluctuate between 2 to 17 cm/ka, and encompass the range of hemipelagic

449   sedimentation rates (5 to 10 cm/ka) previously determined in the area [Reid et al., 1996;

450   Watt et al., 2012b]. The greater variability in apparent accumulation rates determined

451   from Age Model 1 (particularly for the lower sedimentation rates) likely reflects the

452   effects of turbidite erosion. Sedimentation rates in age model 1 between 300-988 ka are

453   relatively constant at 3.2-9 cm/ka. The reduction in variability of sedimentation rates

454   further down the core likely reflects the fact that there are fewer dated horizons deeper in

455   Hole U1395B, resulting in a smoother apparent sedimentation rate.

456

457   **Age Models 2 and 3**: Age Model 2 uses Deposit 2 as a boundary at 130 ka (Figure 2;

458   Cassidy et al., [2015]) at 18.49 m, and the paleomagnetic dates of 781 ka, and 988 ka, at

459   depths of 63.06 m, and 89.08 cm respectively. Age Model 3 uses only the two

460   paleomagnetic dates. Using Age Models 2 and 3, estimated sedimentation rates are less

461   variable throughout the core with long-term rates of 4-8 cm/ka.

462

463   *4.2. Event frequency offshore Montserrat*

464   Events are not distributed regularly through time in core U1395B, but appear to cluster

465   within specific time periods (Figure 4). To better understand this long-term variation in

466   event timing we conduct a moving sum, where the number of events are summed every

467   50 kyr, at 10 kyr increments. Observations do not change when using bins of 30 kyr and

468   100 kyr (see Figures S4 and S5). Conservatively, we classify periods of increased

469   frequency as periods where all three age models show that the frequency of event deposits

470   is above the mean 90% confidence interval of the moving sum data (Figure 5). Periods of

471   reduced activity are defined as periods where all three age models show that event

472   frequency is below 1 standard deviation from the mean. In all age models, these periods

473   of relative quiescence last on the order of 10^4- 10^5 kyr. In Hole U1395B, all age models

474   show an increased frequency of all event deposits (above the 90% confidence interval of

475   8.44 events in 50 ka) between ~170 ka to ~120 ka. This peak in Montserrat's volcanism

476   lies within the period of Soufrière Hills activity (constrained from subaerial dates as 290

477   ka to present, but see discussion in Section 5.1), and suggests that the largest flank

478   collapse of Soufrière Hills (Deposit 2, at 130 ka) and the South Soufrière Hills basaltic

479   episode (~130 ka) both occurred towards the end of the most active phase of Soufrière

480   Hills' eruptive history.

481

482   When examining volcaniclastic deposits only (volcanic turbidites and tephra fall), there

483   are three periods where frequency is greater than the mean 90% confidence interval,

484   between ~930 ka to ~900 ka, ~810 ka to ~760 ka, and ~190 ka to ~120 ka. We interpret

485   periods with a higher frequency of both tephra fall and volcaniclastic turbidites as

486   representing episodes of elevated eruptive activity at Montserrat (Figure 5). The older two

487   periods coincide with activity at Centre Hills volcano, and the younger period (which is

488   similar to that derived from the whole dataset) to Soufrière Hills.

489

490   The periods of heightened volcanic activity show a general correlation with changes in the

491   style of eruptions at Montserrat (Figures 4 and 5). The ~810 to ~760 ka increase in event

492   frequency coincides with the appearance of scoria within Hole U1395B. The ~190 ka to

493   ~120 ka increase in event frequency coincides broadly with the onset of activity at South

494   Soufrière Hills [Harford et al., 2002].

495

496   To test if there is any correlation between sea-level and turbidite frequency we use a

497   linear model (LM), generalised linear model (GLM), and proportional hazards model

498   (PHM) after binning the data into 10 kyr intervals. For further details on the statistical

499   methods see Hunt et al. [2014] and Clare et al. [2016]. Unit ages are given in Table S4

500   and test results are given in Table 2.

501

502   Statistical analyses are conducted on all three age models in order to test the sensitivity of

503   results to dating errors and to determine if the results are artefacts of the specific age

504   model used. By comparing results from the three age models, the effects of age

505   uncertainty can be better understood. We pose the null hypothesis that turbidite frequency

506   is not correlated with sea-level, and P-values < 0.05 allow us to reject this hypothesis.

507   Table 2 shows that using age model 1 does not show significance in any statistical tests,

508   but using age models 2 and 3 shows significance in all three statistical tests. It should be

509   noted, however, that the correlation coefficient for LM is very low (0.002, 0.085, and

510   0.077 for age models 1-3 respectively). Low correlation coefficients for age models 2 and

511   3 indicate that while there may be a broad correlation between sea-level and turbidite

512   frequency, the variation means that the scatter about that trend is very wide. Grouping

513   together of turbidites from eruptive and collapse activity, effects of data binning, or

514   genuine natural noise, may cause this broad scatter. We therefore conclude that all three

515   age models are in agreement and show that there is little to no correlation between sea-

516   level and turbidite frequency. Dating errors are unlikely to affect this observation due to

517   the consistency of this result across all three age models.

518

519   Although there appears to be no correlation between turbidite frequency and sea-level, all

520   three of the dated larger landslide deposits from Soufrière Hills volcano (Deposits 1 and 5,

521 8-14 ka and Deposit 2, 130 ka occur during periods of rapid sea-level rise (>5 m/ka)

522 (Figure 5). Note that older landslides of Centre Hills age are not well dated. Larger

523 landslide deposits, associated with volcanic flank collapse, are easily distinguishable from

524 other eruption-related deposits, unlike turbidites, and there is a better degree of

525 confidence in the dating of these events. We investigate this apparent correlation in a later

526 section using a wider global dataset (*section 5.5.*).

527

528 **5. Discussion**

529

530 *5.1. How does the submarine record relate to subaerial activity?*

531 Montserrat is part of an active island arc with numerous active volcanoes on other islands,

532 which may be the source of some deposits in the U1395B stratigraphy. For example, site

533 U1395B is situated ~25 km southeast of Montserrat and ~35 km downwind (northwest) of

534 Guadeloupe [Radiosonde wind data], which is thus also a plausible potential source for

535 deposits in the core. Eruptive products from Guadeloupe can be distinguished using lead

536 isotopes because Guadeloupe has a higher radiogenic lead component [Cassidy et al.,

537 2012a; Palmer et al., 2016], and Coussens et al. [2016] use Pb isotopes to show that most

538 tephra layers recorded within Hole U1395 B are likely to be from Montserrat. Over the

539 past 1 Ma [Samper et al., 2007], volcanic activity occurred in the southeast of Guadeloupe

540 at Grande Découverte Soufrière, producing landslides that have mostly travelled

541 westwards into a canyon system [Samper et al., 2007]. The canyon system has

542 accumulated deposits towards the west or southwest of Guadeloupe: thus, landslides and

543 turbidites from Guadeloupe are unlikely to produce deposits within Hole U1395B, and we

544 assume that the majority of visible turbidite layers are from Montserrat.

545

546   Limited Ar-Ar dating from on-land samples on Montserrat suggests that volcanism

547   occurred at Centre Hills between ~990–550 ka [Harford et al., 2002] followed by a long

548   hiatus in activity until ~290 ka, when activity commenced at Soufrière Hills. At ~130 ka

549   there was a brief period (~10 kyr) of eruptive activity at the new volcanic centre, South

550   Soufrière Hills, after which activity migrated back to the Soufrière Hills. The apparent

551   gap in subaerial volcanism from ~500-290 ka is not replicated in any of the age models

552   for Hole U1395B (Figures 4 and 5), where the periods of relative quiescence are much

553   shorter, lasting 10^4-10^5 kyr. This suggests that activity migrated relatively rapidly between

554   Centre Hills and Soufrière Hills, and may even have overlapped. This difference between

555   the subaerial and marine records is likely an artefact of limited dating, exposure and

556   erosion of the subaerial record. As such, the offshore stratigraphy provides a higher

557   resolution record and a better means of investigating temporal patterns in volcanic activity

558   in greater detail.

559

560   Trofimovs et al. [2006] showed that 90% of the eruptive products from the 1995-2010

561   eruption of Montserrat had been deposited offshore, supporting our inference that the

562   submarine record is likely to provide a more complete archive of events than the subaerial

563   record. However, deposition in marine settings involves complex transitions between

564   subaerial and submarine transport processes. Thus, although the offshore stratigraphy

565   records more volcanic events than the subaerial record, offshore facies may not provide a

566   truly representative record of a particular type of eruption.

567

568   *5.2. How does the frequency of collapses relate to volcanism?*

569   Increases in the frequency of tephra fall deposits above the mean 90% confidence interval

570   (3.64 events in 50 ka) indicate that there was more explosive volcanic activity between

571   ~800 ka to ~760 ka (Centre Hills period), and ~230 ka to ~140 ka (Soufrière Hills period)

572   (Figure 5). Turbidite frequency also increases during these periods, but not all observed

573   increases are above the mean 90% confidence interval (Figure 5). These observations are

574   consistent for all age models used, suggesting that these periods of increased volcanism

575   and turbidite frequency are unlikely to be age model artefacts. During periods of effusive

576   volcanic activity (i.e. the lava-dome forming eruptions that typify much of Montserrat's

577   volcanism), there is a greater rate of edifice growth and an increase in the number of

578   volcano-tectonic earthquakes and explosive eruptions, all of which are likely to enhance

579   the likelihood of mass wasting. The largest flank collapse from Soufriere Hills (130 ka)

580   occurred near the end of the peak activity at the centre (whether derived from all core

581   deposits, or tephra fall deposits alone), suggesting that elevated output at this time led to

582   major flank instability.

583

584   Bioclastic turbidites show another increase in frequency at ~560 ka to ~500 ka suggesting

585   that other factors may be important in triggering or priming carbonate shelf collapse

586   (Figure 5), such as sea-level change or large earthquakes.

587

588   *5.3. How does the frequency of collapses at Montserrat relate to sea-level?*

589   Turbidite frequency does not show a statistically robust correlation with eustatic sea-level

590   changes (in all age models), but all three of the well-dated large-scale landslides (>0.3

591   km^3) from Montserrat (Deposits 1, 2 and 5) occurred during periods of rapid (>5 m/ka)

592   global sea-level rise (Figure 5) [Miller et al., 2005]. Deposits 1 and 5 (dated between 14-8

593   ka) coincide with rapid sea-level rise at 15 ka to 5 ka, from 60 m to 1.6 m below present

594   day sea-level (Figure 5). Deposit 2 is dated at 130 ka, which coincides with a second

595   period of rapid sea-level rise at 130 ka to 120 ka (Figure 5). Although this is a small

596   number of events, the record suggests that rapid sea-level rise may trigger or precondition

597   the flank collapses on Montserrat.

598

599   *5.4. Large-scale flank collapse: constructing a global landslide record.*

600   To investigate if large landslide occurrences during rapid sea-level rise are replicated

601   more widely, we have compiled a global dataset of landslide ages at volcanic islands over

602   the past 1 Ma, building on the compilation by Quidelleur et al., [2008]. The compiled

603   global data set has 25 ages from volcanic islands (errors <±22.5 ka) that are constrained

604   within errors of ±22.5 ka, comprising 9 from ocean islands and 16 from island arcs

605   (Tables 3 and 4).

606

607   Many landslides have large age uncertainties, and if age errors are too large (i.e., on the

608   order of sea-level cycles) then relationships between sea level, volcanism, and landslides

609   cannot be determined [Pope et al., 2015]. Our age-uncertainty criterion of <± 22.5 ka has

610   been selected on this basis, because it provides a sufficiently large dataset to observe

611   potential patterns, with age errors that are a similar order of magnitude to the periodicity

612   of sea-level cycles (10^3-10^4 yrs).

613

614   *5.4.1 Ocean islands*

615   Multiple large-scale landslide deposits dating back to at least 22 Ma lie offshore the

616   Canary Islands [Stillman, 1999]. The oldest well-dated landslide from the island of El

617   Hierro is El Julan, to the SW (130 km^3) [Gee et al., 2001]. Onshore there is an 8 km wide

618   scar, with infilling material dated at <158 ± 4 ka [Guillou et al., 1996]. Turbidite P, in the

619   Madeira Abyssal Plain, is dated at 540 ± 10 ka using biostratigraphy, and is correlated to

620   the El Julan landslide based on geochemistry and subaerial date constraints [Hunt et al.,

621   2013], and is our best age estimate of the El Julan collapse. North of El Hierro lies the El

622   Golfo deposit (150 km^3) [Urgeles et al., 1997], which is correlated with a large (14.5 km

623   wide) subaerial crater [Urgeles et al., 1997]. This scar is dated between 87± 8 ka and 11 ±

624   7 ka using Ar-Ar dating of material that are incised by and infill the scar [Guillou et al.,

625   1996]. In the Madeira Abyssal Plain turbidite B is correlated with the El Golfo collapse

626   [Hunt et al., 2013] and is dated at 15 ± 5 ka [Weaver et al., 1992; Hunt et al., 2013] using

627   biostratigraphy of surrounding hemipelagic material. We use the age of turbidite B for the

628   date of the El Golfo collapse in this study.

629

630   The Icod, Orotava and Guimar landslides are the best-dated landslides from Tenerife. The

631   Guimar landslide (120 km^3) [Krastel et al., 2001] correlates with turbidite Z in the

632   Madeira Abyssal Basin [Hunt et al., 2013], which places the events via biostratigraphic

633   ages at 850±10 ka. The Orotava and Icod landslides, north of Tenerife, correlate with

634   large amphitheatre-shaped depressions. The minimum age of the Orotava landslide is

635   deduced from the oldest lava flow (PS4) infilling the Orotava Valley (534±9 ka)

636   [Boulesteix et al., 2013], and the maximum age from lavas intersected by the landslide

637   scar (558±8 ka). The landslide also correlates with turbidite MO in the Madeira Abyssal

638   Plain, dated at 540±5 ka using biostratigraphy [Hunt et al., 2013]. Subaerial dating

639   suggests the Icod landslide occurred between 175±3 ka and 161±5 ka by K-Ar dating

640   material that are incised by and infill the landslide scar respectively [Boulesteix et al.,

641   2011] but more recently Hunt et al., [2013] used turbidite G in the Madeira Abyssal Plain

642   to obtain a biostratigraphic age of 165±5 ka, which we use here.

643

644   Offshore La Palma, the Cumbre Nueva landslide is well-dated. The headwall of the

645   landslide has been identified as the prominent Cumbre Nueva Ridge that encloses a

646   horseshoe-shaped depression [Urgeles et al., 1999]. The Cumbre Nueva landslide is

647   thought to have occurred after the emplacement of the Upper Taburiente volcanic deposits

648   (566±8 ka) and was followed by the emplacement of the Bejenado volcano (537±8 ka) in

649   the landslide scar [Guillou et al., 1998, 2001; Carraceado et al., 2001]. Hunt et al [2013]

650   date the Cumbre Nueva landslide at 480±5 ka by correlating the landslide with turbidite N

651   in the Madeira Abyssal Plain. This contrasts with subaerial dating, and we preferentially

652   use the subaerial dates, because turbidite N may correlate with a younger landslide from

653   La Palma.

654

655   To the east of Pico del Fogo in the Cape Verde Islands is a 130-160 km^3 landslide deposit

656   [Lebas et al., 2007; Masson et al., 2008], which has been correlated with fields of

657   boulders and chaotic conglomerates (interpreted as tsunami deposits) on the nearby island

658   of Santiago [Ramalho et al., 2015]. ^{3}He dating of these tsunami deposits suggests a

659   landslide age of 73±7 ka [Ramalho et al., 2015]. This is close in age to a post collapse

660   lava flow on Pico del Fogo dated at 86±3 ka [Paris et al., 2011].

661

662   In the Hawaiian Archipelago at least 68 large volume landslides (up to 5000 km^3) have

663   been identified [Moore et al., 1989, 1994]. However, only the Alika 2 deposit, offshore

664   Mauna Loa, is well dated. Cores F88 B-13, F91 39B1 and F91 4082 sample the Alika 2

665   deposit. Planktonic forams within the Alika 2 deposit date the landslide at 127±5 ka using

666   oxygen isotope stratigraphy [McMurty et al., 1999].

667

668   The island of Tahiti has two horseshoe shaped depressions to the north and south of the

669   island that correlate with large hummocky landslide deposits offshore with respective

670   volumes of 800 km^3 and 1150 km^3 [Hildenbrand et al., 2004]. The Tahitian shield was

671   constructed between 1.4-8.7 Ma [Hildenbrand et al., 2004], with vent locations

672   concentrated along an E-W rift down the centre of the island. Late activity along these

673   vents (~870 ka) is thought to have triggered the two landslides [Hildenbrand et al., 2004].

674   After the landslides, activity moved to the north, infilling the northern crater (851±11 ka)

675   [Hildenbrand et al., 2004]. We therefore assume an age range for the northern landslide

676   between 870 to 851±11 ka. The southern crater is dated at ~500 ka, but is too poorly

677   constrained to be included in the database.

678

679   *5.4.2 Island Arc Landslides*

680   Evidence of large landslides has been identified at several islands in the Lesser Antilles

681   (in addition to Montserrat). At Guadeloupe, subaerial exposures allow two events, the

682   Carmichael and Carbet landslides, to be well dated [Boudon et al., 1984, 1987, 2007]. The

683   Carmichael landslide covers 17 km^2 onshore, and large blocky deposits are observed

684   offshore [Boudon et al., 1984]. The landslide is thought to be associated with the

685   Carmichael crater that has a volume of 0.3 km^3. Uncarbonised wood found within the

686   deposit yields ^{14}C ages of 8400 ±1500 to 11270±185 BP [Boudon et al., 1984]. The

687   Carbet landslide (estimated volume of 0.5 km^3) is dated by subaerial outcrops along the

688   Rivière du Carbet, where uncarbonised wood within the deposits yielded ^{14}C dates

689   between 2800-3450 BP [Boudon et al., 1984, 2007; Daigun et al., 1981].

690

691   On Dominica four large landslides are observed, but only the Soufriere event is well dated.

692   The Soufriere event (estimated volume 6-7 km^3) formed from the collapse of the Plat

693   Pays volcanic edifice [Le Friant et al., 2002]. The lower bound age constraint is from ^{14}C

694   dating of carbonaceous material found within a pyroclastic flow deposit from the Plat-

695   Pays volcano dated at 6600±50 ka. An upper bound comes from ^{14}C dating material

696   (2380± 75 ka) from a tephra fall that overlies a mega block from the landslide (Scotts

697   Head) [Le Friant et al., 2002].

698

699   On Martinique, three of the four large landslide deposits are well dated (D1, D2 and D3).

700   The D1 event is associated with a large west-facing landslide scar and has an estimated

701   volume of 25 km^3. The northern rim of the crater is well exposed, but the southern rim

702   may have been destroyed and/or covered by later landslide events [Boudon et al., 2007].

703   K-Ar dating of material infilling and incised by the landslide scar are dated at 126±2 ka

704   and 127±2 ka respectively. The D2, or St Pierre event formed a large west-facing

705   amphitheatre-shaped structure and produced an offshore deposit with a volume of >13

706   km^3. The upper bound date is given by U-Th disequilibrium dating of material

707   intersected/outside the D2 structure, yielding ages of 37±4 ka (Mont Calebasse lava

708   dome) and 25±1 ka (Mourne Plumé lava dome) [Le Friant et al., 2003]. The lower bound

709   age, of 25 000±1040 years, is given by a ^{14}C charcoal age from a scoria flow deposit that

710   in-fills the D2 structure [Vincent et al 1989]. D3, or the Rivière Sèche event, has an

711   estimated volume of 2 km^3. The Aileron lava dome (summit part of Montagne Pelée) is

712   intersected by the D3 structure and is dated at 9.7±0.5 ka, providing an upper age limit

713   [Le Friant et al., 2003]. The "Sans Nom" lava dome in-fills the D3 structure and is dated

714   at 9±1 ka [Le Friant et al., 2003].

715

716   Further afield, multiple large landslide deposits have been identified on and offshore

717   Ischia, Italy [Chiocci and de Alteriis 2006; De Alteriis and Violante, 2009], five of which

718   are well dated. The South landslide (1.5 km^3) is correlated with the offshore DF1 deposit

719   and is dated at 2.4-3 ka (^{14}C on planktonic forams within hemipelagic material above and

720   below DF1) [De Alteriis et al., 2010]. The Falanga and Pietre Rosse landslides outcrop to

721   the east of Ischia, with a combined offshore volume of 11 km^3. The Falanga deposit is

722   dated at 400 BC based on historical chronicles [Buchner 1986]. The Pietre Rosse

723   landslide has a maximum age constraint as it overlies the Citara Formation 40 ka [Vezzoli

724   1988], and the upper bound age is given by the overlying Falanga landslide.

725

726   To the north of Ischia two large landslide deposits (NDDe and NDDw) are seen [De

727   Alteriis and Violante 2009]. The NDDe correlates onshore with the Casamicciola and

728   Lacco Ameno landslide deposits [Seta et al., 2012]. The Lacco Ameno deposit is poorly

729   dated and is not included within the global database. The Casamicciola deposit overlies

730   the Punta La Scrofa Tuff, dated at <800 BC [De Vita et al., 2010]. Within seismic

731   reflection profiles, a horizon beneath NDDw has been correlated with the onshore Zaro

732   lava flow, dated at 6±2 ka and 9±1 ka using K-Ar dating [Vezzoli et al., de Aleriis and

733   Violante, 2009]. Although the Casamicciola and NDDw have no upper bounds, the ages

734   are within the error of ± 22.5 kyr, and so are included within the global dataset.

735

736   The Japanese volcano of Usu is situated in the South of the Japanese island of Hokkaido.

737   Usu formed ~20 ka [Soya et al., 2007] and after the edifice reached 1000 m there was a

738   large summit collapse (1-2 km^3). This collapse, named the Zenkojii collapse, occurred at

739   ~7-8 ka based on subaerial dating of infilling and cross-cut deposits [Moriya, 2003 (in

740   Japanese); Soya et al., 2007].

741

742   A large 5 km^3 collapse from Ritter island (offshore New Guinea), which occurred 13th

743   March 1888, is also included in the global database [Cooke 1981; Ward and Day 2003].

744

745

746   *5.5. Large-scale flank collapse and sea-level: comparison to global records*

747   At Montserrat, the three well-dated large landslides from Soufrière Hills coincide with

748   periods of rapid sea level rise. Using the global compilation, box and whisker plots

749   (Figure 6) show that landslide occurrences at other island volcanoes are skewed towards

750   periods of more rapid sea-level rise. In contrast, at ocean islands the distribution of event

751   timing shows no clear correlation with specific regimes of sea level (Figure 6). This is

752   supported by preliminary statistical analyses (Mann-Whitney and Kolmogorov-Smirnov

753   tests, see supplementary information).

754

755   The global data set of landslide ages is restricted (9 events from ocean islands, 16 events

756   from island arcs). Dating landslide deposits is challenging, because most material is

757   emplaced offshore in poorly accessible, deep marine settings, typically comprising

758   chaotic mixtures of material. Direct dating of material within landslides only provides

759   maximum age constraints of landslide emplacement, unless material such as vegetation

760   incorporated into the landslide deposits can be identified and dated. Indirect dating of

761   material overlying and underlying landslide deposits or scars can result in large age gaps.

762   Consequently the global landslide database is sparse, and dominated by a very few well-

763   studied regions (e.g. Ischia, Lesser Antilles). Even in other regions where numerous

764   events have been identified (e.g. Aleutian Islands; Coombs et al. [2007]), very few events

765   are dated, and so are excluded from our dataset.

766

767   Given the limitations of a restricted dataset, it is thus difficult to test the strength of the

768   observed correlation between event timing and sea level change. Furthermore the island

769   arc database is biased towards recent landslide events (<20 ka), which includes a period

770   of rapid sea-level rise (Figure 6). Thus the apparent prevalence of island arc landslides

771   during periods of rapid sea-level rise could also be affected by a temporal record bias.

772   Further investigation (by substantially increasing the dated landslide database) is required

773   to test this initial result, which suggests a difference between how sea level change

774   influences flank stability in island arc and ocean island settings.

775

776   Nevertheless, it is worth briefly considering the processes by which sea level rise may

777   increase the likelihood of flank collapse at island-arc volcanoes. A ~100 m rise in sea

778   level potentially enhances both dyke ascent (and hence volcanism) and fault movement in

779   island-arc settings [cf. Nakada and Yokose, 1992], although the relationship between

780   volcanism and sea level change may be complex [McGuire et al., 1997] and is

781   incompletely understood. Overpressure in magma chambers, which decreases by

782   viscoelastic relaxation, is more sensitive to loading rate than the absolute load [Jellinek et

783   al., 2004] consistent with the observed correlation of collapse rapid sea-level rise.

784   Furthermore, sealevel rise may result in greater magma- water interaction encouraging

785   explosive, phreatomagmatic behaviour. Such explosive behaviour may reduce flank

786   stabitlity. An incipient instability within a volcanic edifice may also move closer to a

787   critical failure point due either to direct stress increases associated with sea-level rise,

788   possibly combined with other factors. These may include enhanced erosion and

789   modification of the groundwater system associated with rapid sea-level change. Although

790   the consequence of sea-level rise on groundwater may depend on local factors, pore-

791   pressure increases within hydrothermal systems have been suggested as a cause of edifice

792   collapse [Elsworth and Voight, 1995; Day, 1996; Reid, 2004].

793

794   Our results suggest that these factors may be less significant in ocean-island settings, but

795   the reason for this is as yet unclear. Structurally, the more basaltic composition of ocean

796 islands means they are likely to have more stable flanks than island arcs, with a broader

797 profile and lower slope gradients [Watt et al., 2014], yet the presence of widespread

798 landslide deposits around many ocean islands indicates that they are still prone to

799 catastrophic flank failure.

800

801

802 **6. Conclusions**

803

804 In contrast to the subaerial stratigraphic record, volcaniclastic layers within IODP Hole

805 U1395B provide a more complete record of volcanism on Montserrat. Periods of reduced

806 event frequency (interpreted as periods of volcanic quiescence) last of the order $10^4 - 10^5$

807 ka, substantially less than apparent gaps in the subaerial record. The pauses in activity

808 suggested by the subaerial record are likely to be a manifestation of poor preservation and

809 burial of onshore stratigraphy, coupled with the predominantly offshore deposition of

810 volcanic products. The marine record reveals that three periods of heightened volcanic

811 activity at Montserrat occurred at ~930 ka to ~900 ka, ~810ka to ~760 ka (both during the

812 Centre Hills period), and ~190 ka to ~120 ka (during the Soufrière Hills period). A

813 notable increase in event frequency at ~810 ka to ~760 ka coincides with the occurrence

814 of mafic scoria in Hole U1395B, while the peak in Soufrière Hills volcanism coincides

815 with the largest flank collapse from the volcano (130 ka) and a brief switch to mafic

816 volcanism.

817

818 Periods of heightened volcanic activity coincide with periods of increased turbidite

819 occurrence, suggesting that intensified volcanic activity may facilitate mass-wasting

820 processes. No statistically significant correlation of turbidite occurrence (collapse

821   frequency) and sea level were observed, but all of the well-dated and large-scale

822   landslides on Montserrat occurred during periods of rapid sea-level rise. While the global

823   dataset is small and there are uncertainties associated with dating landslide events, this

824   pattern of large-scale landslides coinciding with periods of rapid sea-level rise is

825   replicated within a global data set for island-arc volcanoes, but not at ocean islands. The

826   reasons for this difference between island arcs and ocean islands remain unclear, but may

827   reflect a greater susceptibility of the steeper, more lithologically diverse flanks of island-

828   arc volcanoes to rapid sea-level changes, relative to ocean islands.

829

844

845   **8. References**

846

847   Ablay, G. J. and J. Marti (2000), Stratigraphy, structure, and volcanic evolution of the

848   Pico Teide-Pico Viejo formation, Tenerife, Canary Islands, *Journal of Volcanology*

849   *and Geothermal Research, 103*, 175-208

850

851   Ancochea, E., J. M. Fuster, E. Ibarrola, A. Cendrero, J. Coello, F. Hernan, J. M. Cantagrel,

852   C. Jamond (1990), Evolution of the island of Tenerife (Canary Islands) in the light of

853   new K-Ar data, *Journal of Volcanology and Geothermal Research*, 44, 231-249, doi:

854   0377-0273/90/$03.50

855

856   Boudon, G., M. P. Semet, and P. M. Vincent (1984), Flank failure–directed blast eruption

857   at Soufrière, Guadeloupe, French West Indies: A 3,000-yr-old Mt. St. Helens?, *Geology*,

858   *12*(6), 350-353

859

860   Boudon, G., M. P. Semet, and P. M. Vincent (1987), Magma and hydrothermally driven

861   sector collapses: The 3100 and 11,500 y. BP eruptions of la Grande Decouverte (la

862   Soufrière) volcano, Guadeloupe, French West Indies, *Journal of volcanology and*

863   *geothermal research*, *33*(4), 317-323

864   Boudon, G., A. Le Friant, J. C. Komorowski, C. Deplus and M. P. Semet (2007), Volcano

865   flank instability in the Lesser Antilles Arc: Diversity of scale, processes, and

866   temporal recurrence, *Journal of Geophysical Research, 112*, B08205,

867   doi:10.1029/2006JB004674

868   Boulesteix. T., A. Hildenbrand, P-Y. Gillot and V. Soler (2011), Eruptive response of

869   oceanic islands to giant landslides: New insights from the geomorphologic evolution

870 of the Teide–Pico Viejo volcanic complex (Tenerife, Canary), *Geomorphology,*

871 *138,61-73*

872 Buchner, G. (1986), Eruzioni vulcaniche e fenomeni vulcano-tettonici di età preistorica e

873 storica nell' isola di Ischia, *In Tremblements de terre, éruptions volcaniques et vie*

874 *des hommes dans la Campanie antique, vol, 7,* edited by C. Albore-Livadie,

875 *Publishe by Centre Jean Bérard*, Napoli, 145–188

876 Cande, S.C., D. V. Kent, 1992a. A new geomagnetic polarity time scale for the Late

877 Cretaceous and Cenozoic, *Journal of Geophysical Research* 97, 13917-13951

878 Cande, S.C., D. V. Kent, 1992b, Ultrahigh resolution of marine magnetic anomaly

879 profiles: A record of continuous paleointensity variations?, *Journal of Geophysical*

880 *Research* 97, 15075-15083

881 Cande. S. C., D. V. Kent (1995), Revised calibration of the geomagnetic polarity

882 timescale for the Late Cretaceous and Cenozoic, *Journal of Geophysical Research,*

883 *100(B4),* 6093-6095

884 Carracedo, J. C. (1999), Growth, structure, instability and collapse of Canarian volcanoes

885 and comparisons with Hawaiian volcanoes, *Journal of Volcanology and Geothermal*

886 *Research,* 94(1), 1–19.

887 Cassidy, M., R. N. Taylor., M. R. Palmer., R. Cooper., C. Stenlake., J. Trofimovs (2012a)

888 Tracking the magmatic evolution of an island arc volcano: Insights from a high-

889 precision Pb isotope record of Montserrat, Lesser Antilles, *Geochemistry,*

890 *Geophysics, Geosystems,* 13, Q05003 doi:10.1029/2012GC004064

891 Cassidy, M., J. Trofimovs, S. F. L. Watt, M. R. Palmer, R. N. Taylor, T. M. Gernon, P.J.

892   Talling and A. Le Friant (2012b), Multi-stage collapse events in the South Soufrière

893   Hills, Montserrat, as recorded in marine sediment cores, *In the eruption of Soufrière*

894   *Hills Volcano, Montserrat from 2000-2010,* Edited by G. Wadge, G., et al., *The*

895   *Geological Society Special Publications*, *39*, 383-397

896 Cassidy, M., J. Trofimovs, M. R. Palmer, P. J. Talling, S. F. L. Watt, S. G. Moreton and

897   R. N. Taylor (2013), Timing and emplacement dynamics of newly recognised mass

898   flow deposits at ~8-12 ka offshore Soufrière Hills volcano, Montserrat: How

899   submarine stratigraphy can complement subaerial eruption histories, *Journal of*

900   *Volcanology and Geothermal Research, 253,* 1–14,

901   doi:10.1016/j.jvolgeores.2012.12.002

902 Cassidy, M., S. F. L. Watt, M. R. Palmer, J. Trofimovs, W. Symons, S. E. Maclachlan and

903   A. J. Stinton (2014), Construction of volcanic records from marine sediment cores: A

904   review and case study (Montserrat, West Indies), *Earth-Science Reviews, 138*, 137–

905   155, doi:10.1016/j.earscirev.2014.08.008

906 Cassidy. M., et al., (2015), Rapid onset of mafic magmatism facilitated by volcanic

907   edifice collapse, *Geophysical Research Letters, 42(12),* 4778-4785

908 Clare, M. A, P. J. Talling, P. H. Challenor and J. E. Hunt, (2016). Tempo and triggering

909   of large submarine landslides - Statsitical analysis for hazard assessment. In

910   Submarine Mass Movements and Their Consequences, edited by G. Lamarche et

911   al., . Springer, 41, 509-517

912

913 Cole, P. D., E. S. Calder, R. S. J. Sparks, A. B. Clarke, T. H. Druitt, S. R. Young and G.

914   E. Norton (2002), Deposits from dome-collapse and fountain-collapse pyroclastic

915   flows at Soufrière Hills Volcano, Montserrat, G*eological Society, London, Memoirs,*

916   21(1), 231-262

917 Collins, B. D. and T. Dunne (1986), Erosion of tephra from the 1980 eruption of Mount

918   St. Helens, *Geological Society of America Bulletin*, *97*(7), 896-905

919 Cooke, R.J.S. (1981), Eruptive history of the volcano at Ritter Is- land, in Cooke–Ravian

920   Volume of Volcanological Papers, *In Geological Survey of Papua New Guinea*

921   *Memoir*, edited by R. W. Johnson, 10, 115-123

922 Coombs, M. L., S. M. White and D. W. Scholl, (2007), Massive edifice failure at Aleutian

923   arc volcanoes, *Earth and Planetary Science Letters,* 256(3), 403-418

924 Coussens M, et al., (2016), Synthesis: stratigraphy and age control for IODP Sites U1394,

925   U1395, and U1396 offshore Montserrat in the Lesser Antilles. *In Proceedings of the*

926   *Integrated Ocean Drilling Program,* principal investiagators A. Le Friant, O.

927   Ishizuka, N. A. Stroncik, Volume 340

928 Crutchley, G. J., J. Karstens, C. Berndt, P. J. Talling, S. F. L. Watt, M. E. Vardy, V.

929   Huhnerbach, M. Urlaub, S. Sarkar, D. Klaeschen, M. Paulatto, A. Le Friant, E. Lebas

930   and F. Maeno (2013), Insights into the emplacement dynamics of volcanic landslides

931   from high-resolution 3D seismic data acquired offshore Montserrat, Lesser Antillies,

932   *Marine Geology, 335*,1-15, doi:10.1016/j.margeo.2012.10.004

933 Dagain, J. (1981), La mise en place du massif volcanique Madaleine—Soufrière, Basse-

934   Terre de Guadeloupe, Antilles [3rd cycle thesis]: Orsay, France, Université Paris Sud

935   Dagain, J., M. Paterne, and D. Westercamp (1981), La mise en place du massif

936   Madeleine-Soufrière, Basse-Terre de Guadeloupe, A*ntilles: Académie des Sciences,*

937   *Comptes Rendus*, 11 (292), 921-926

938   Day, S. J. (1996), Hydrothermal pore fluid pressure and the stability of porous, permeable

939   volcanoes. *In Volcano Instability on the Earth and Other Planets*, edited by W. J.

940   McGuire, A. P. Jones, *Geological Society Special Publication*, 110, 77-93

941   De Alteriis, G. and C. Violante (2009), Catastrophic landslides off Ischia volcanic island

942   (Italy) during prehistory, *Geological Society, London, Special Publications*, 322(1),

943   73-104

944   De Alteris, G., D. D. Insinga, S. Morabito, V. Morra, F. L. Chiocci, F. Terrasi, C.

945   Lubritto, C. Di Benedetto and M. Pazzaneses (2010), Age of submarine debris

946   avalanches and tephrostratigraphy offshore Ischia Island, Tyrrhenian Sea, Italy,

947   *Marine Geology,* 278, 1-18, doi:10.1016/j.margeo.2010.08.004

948   Deplus, C., A. Le Friant, G. Boudon, J. C. Komorowski, B. Villement, C. Harford, J.

949   Segoufin and J. L. Chiminee (2001), Submarine evidence for large-scale debris

950   avalanches in the Lesser Antillies Arc, *Earth and Planetary Science Letters, 192,*

951   145-157

952   De Vita, S., F. Sansivero, G. Orsi, E. Marotta and M. Piochi (2010), Volcanological and

953   structural evolution of the Ischia resurgent caldera (Italy) over the past 10 ky.

954   *Geological Society of America Special Papers*, 464, 193-239

955   Elsworth. D and B. Voight, (1995), Dike intrusion as a trigger for large earthquakes and

956   the failure of volcano flanks, *Journal of Geophysical Research*, 100, 6005-6024

957   Folk, R. L. and W. C. Ward (1957), Brazos River bar: a study in the significance of grain

958   size parameters, *Journal of Sedimentary Petrology, 27,* 3-26

959   Gee, M. J. R., D. G. Masson, A. B. Watts and P. A. Allen (2001), The Saharan Debris

960   Flow: an insight into the mechanics of long runout debris flows, *Sedimentology*, 46,

961   317-335

962   Gee, M. J. R., A. B. Watts, D. G. Masson and N. C. Mitchell (2001), Landslides and the

963   evolution of El Hierro in the Canary Islands, *Marine Geology*, 177, 271-293

964   Germa, A., X. Quidelleur, S. Labanieh, P. Lahitte and C. Chauvel (2010), The eruptive

965   history of Morne Jacob volcano (Martinique Island, French West Indies):

966   Geochronology, geomorphology and geochemistry of the earliest volcanism in the

967   recent Lesser Antilles arc, *Journal of Volcanology and Geothermal Research, 198(3-*

968   *4),* 297–310, doi:10.1016/j.jvolgeores.2010.09.013

969   Germa. A., X. Quidelleur, P. Lahitte, S. Labanieh, C. Chauvel (2011), The K-Ar

970   Cassignol-Gillot technique applied to wester Martinique lavas: A record of Lesser

971   Antilles arc activity from 2 Ma to Mount Pelee volcanism, *Quaternary Geology*, 6,

972   341-355

973   Green, S.B. (1991), How many subjects does it take to do a regression analysis? *In*

974   *Multivariate Behavioral Research*, 26, 499-510.

975   Guillou, H., J. C. Carracedo, F. P. Torrado, and E. R. Badiola (1996), K-Ar ages and

976   magnetic stratigraphy of a hotspot-induced, fast grown oceanic island: El Hierro,

977   Canary Islands, *Journal of Volcanology and Geothermal Research*, 73(1), 141-155

978   Guillou, H., J. C. Carracedo and S. J. Day (1998), Dating of the upper Pleistocene–

979   Holocene volcanic activity of La Palma using the unspiked K–Ar technique, *Journal*

980   *of Volcanology and Geothermal Research*, 86(1), 137-149

981   Guillou, H., J. C. Carracedo and R. A. Duncan(2001), K–Ar, 40 Ar–39 Ar ages and

982   magnetostratigraphy of Brunhes and Matuyama lava sequences from La Palma

983   Island, *Journal of Volcanology and Geothermal Research*, 106(3), 175-194

984   Hatfield. R. and Expedition 340 Scientists (2013), Paleomagnetism in methods, *In*

985   *Proceedings of IODP, 340: Tokyo (Integrated Ocean Drilling Program Management*

986   *International, Inc.),* Edited by A. Le Friant, O. Ishizuka, N. A. Stroncik, and the

987   Expedition 340 Scientists, doi:10.2204/iodp.proc.340.102.2013

988   Harford, C. L., M. S. Pringle, R. S. J. Sparks and S. R. Young (2002), The volcanic

989   evolution of Montserrat using 40Ar/39Ar geochronology, *Geological Society,*

990   *London, Memoirs*, *21*, 93–113, doi: 10.1144/GSL.MEM.2002.021.01.05

991   Herd, R.A., M. Edmonds and V. Bass (2006). Catastrophic lava dome failure at Soufriere

992   Hills Volcano, Montserrat 12–13 July 2003, *Journal of Volcanology and Geothermal*

993   *Research*, 148, 234–252

994   Hildenbrand. A., Gillot. P-Y., Le Roy. I. (2004). Volcano-tectonic and geochemical

995   evolution of an oceanic intra-plate volcano: Tahiti-Nui (French Polynesia), *Earth*

996   *and Planetary Science Letters*, 217, 349-365

997   Houghton, B. F., C. J. N. Wilson, M. O. McWilliams, M. A. Lanphere, S. D. Weaver, R.

998   M. Briggs and M. S. Pringle (1995), Volcanic Zone , New Zealand Chronology and

999   dynamics of a large silicic magmatic system : Central Taupo Volcanic Zone , New

1000 Zealand, *Geology, 23*, 13–16, doi:

1001 10.1130/00917613(1995)023<0013:CADOAL>2.3.CO;2

1002 Hunt, J. E., R. B. Wynn, P. J. Talling and D. G. Masson (2013), Turbidite record of

1003 frequency and source of large volume (>100 km^3) Canary Island landslides in the

1004 last 1.5 Ma: Implications for landslide triggers and geohazards, *Geochemistry,*

1005 *Geophysics, Geosystems*, *14(7)*, 2100–2123, doi: 10.1002/ggge.20139

1006 Hunt, J. E., P. J. Talling, M. Clare, I. Jarvis, and R. B. Wynn (2014), Long-term (17 Ma)

1007 turbidite record of the timing and frequency of large flank collapses of the Canary

1008 Islands, *Geochemistry, Geophysics, Geosystems, 15,*3322–3345, doi:

1009 10.1002/2014GC005232

1010 Jellinek, A.M., M. Manga, and M.O. Saar (2004) Did melting glaciers cause volcanic

1011 eruptions in eastern California? Probing the mechanics of dike formation, *Journal of*

1012 *Geophysical Research*, 109, B09206, doi:10.1029/2004JB002978.

1013 Jutzeler, M., J. D. L. White, P. J. Talling, M. McCanta, S. Morgan, A. Le Friant and O.

1014 Ishizuka (2014), Coring disturbances in IODP poston cores with implication for

1015 offshore record of volcanic events and the Missoula megafloods *Geochemistry,*

1016 *Geophysics, Geosystems,* 3572-3590, doi: 10.1002/2014GC005447

1017 Kameo, K. and T. J. Bralower (1998), Neogene calcareous nannofossil biostratigraphy of

1018 sites 998, 999, and 1000, Caribbean Sea, *Proceedings of the Ocean Drilling*

1019 *Program, Scientifc Results*, *165*,3–17

1020   Keefer, D. K. (2000), Statistical analysis of an earthquake-induced landslide

1021   distribution—the 1989 Loma Prieta, California event, *Engineering Geology*, 58(3),

1022   231-249

1023   Kokelaar, B. P. (2002), Setting, chronology and consequences of the eruption of Soufrière

1024   Hills Volcano, Montserrat (1995-1999). I*n the eruption of Soufrière Hills volcano,*

1025   *Montserrat, from 1995 to 1991*, edited by T. Druitt, and P. Kokelaar, *Geological*

1026   *Society Special Publications, 21*,1–43, doi: 10.1144/GSL.MEM.2002.021.01.02

1027   Krastel, S., H. U. Schmincke, C. L. Jacobs, R. Rihm, T. P. Le Bas, and B. Alibés (2001),

1028   Submarine landslides around the Canary Islands, *Journal of Geophysical Research*,

1029   106 (B3), 3977-3997, doi: 2000JB900413. 0148-0227/01/2000 JB900413$09.00

1030   Lebas, E., S. F. L. Watt, P. J. Talling, N. Feuillet, C. Deplus, C. Berndt and M. Vardy

1031   (2011), Multiple widespread landslides during the long-term evolution of a volcanic

1032   island: Insights from high-resolution seismic data, Montserrat, Lesser Antilles,

1033   *Geochemistry Geophysics Geosystems*, *12(5)*, Q05006, doi:10.1029/2010GC003451

1034   Le Friant, A., Boudon, G., Komorowski, J.-C., Deplus, C. (2002), L'île de la Dominique,

1035   à l'origine des avalanches de débris les plus volumineuses de l'arc des Petites

1036   Antilles, *C.R. Geosci*, 334, 235–243

1037   Le Friant, A., G. Boudon, C. Deplus and B. Villement (2003), Large-scale flank collapse

1038   events during the activity of Montagne Pelée, Martinique, Lesser Antilles, *Journal of*

1039   *Geophysical Research, 108 (B1)*, 2055, doi:10.1029/2001JB001624

1040   Le Friant, A., E. J. Lock, M. B. Hart, G. Boudon, R. S. J. Sparks, M. J. Leng, C. W.

1041   Smart, J. C. Komorowski, C. Deplus, J. K. Fisher (2008), Late Pleistocene

1042 tephrochronology of marine sediments adjacent to Montserrat, Lesser Antilles

1043 volcanic arc, *Journal of the Geological Society*, *165(1)*, 279–289, doi:10.1144/0016-

1044 76492007-019

1045 Le Friant, A., C. Deplus and G. Boudon (2009), Submarine deposition of volcanicastic

1046 material from the 1995-2005 eruptions of Soufrière Hills volcano, Montserrat,

1047 *Journal of the Geological Society, 166*, 171-182, doi: 10.1144/0016-76492008-047

1048 Le Friant, A., C. Deplus, G. Boudon, N. Feuliiet, J. Trofimovs, J. C. Komorowski, R. S. J.

1049 Sparks, P. J. Talling, S. Loughlin, M. R. Palmer and G. Ryan (2010), Eruption of

1050 Soufrière Hills (1995- 2009) from an offshore perspective: Insights from repeated

1051 swath bathymetry surveys, *Geophysical research letters*, *37*, L11307,

1052 doi:10.1029/2010GL043580

1053 Le Friant, A., E. Lebas, V. Clement, G. Boudon, C. Deplus, B. de Voogd and P.

1054 Bachélery (2011), A new model for the evolution of la Reunion volcanic complex

1055 from complete geophysical surveys, *Geophysical Research Letters, 38,* L09312,

1056 doi:10.1029/2011GL047489

1057 Le Friant, A., O. Ishizuka, N. A. Stroncik, A. L. Slagle, S. Morgan, T. Adachi, M.

1058 Aljahdali and G. Boudon (2012), Lesser Antillies Volcanism and Landslides.

1059 Implications for hazard assessment and long-term magmatic evolution of the arc,

1060 *Integrated Ocean Drilling Program, Expedition 340 preliminary report,*

1061 doi:10.2204/iodp.pr.340.2012

1062 Le Friant, A., et al., (2015), Submarine record of volcanic island construction and collapse

1063 in the Lesser Antilles arc: First scientific drilling of submarine volcanic island

1064   landslides by IODP Expedition 340, *Geochemistry, Geophysics, Geosystems, 16*,

1065   420–442, doi:10.1002/ 2014GC005652

1066   Lehmann, E. L. and H. J. D'Abrera (2006), Nonparametrics: statistical methods based on

1067   ranks, *Springer,* 464, New York

1068   Lénat, J, F., P. Boivin, C. Deniel, P. Y. Gillot, P. Bachèlery, and Fournaise 2 Team

1069   (2009), Age and nature of deposits on the submarine flanks of Piton de la Fournaise

1070   (Reunion Island), *Journal of Volcanology and Geothermal Research*, 184, 199–207

1071   Lisiecki, L. E. and M. E. Raymo (2005), A Pliocene-Pleistocene stack of 57 globally

1072   distributed benthic δ^{18}O records, *Paleoceanography*, *20*,1–17,

1073   doi:10.1029/2004PA001071

1074   Longpré, M. A., J. P. Chadwick, J. Wijbrans and R. Iping (2011), Age of the El Golfo

1075   debris avalanche, El Hierro (Canary Islands): New constraints from laser and furnace

1076 ^{40}Ar/^{39}Ar dating, *Journal of Volcanology and Geothermal Research, 203*, 76-80,

1077   doi:10.1016/j.jvolgeores.2011.04.002

1078   Major, J. J., T. C. Pierson., R. L. Dinehart and J. E. Costa (2000), Sediment yield

1079   following severe volcanic disturbance—a two-decade perspective from Mount St.

1080   Helens, *Geology*, 28(9), 819-822

1081   Marques, R., J. Zêzere., R. Trigo., J. Gaspar and I. Trigo (2008), Rainfall patterns and

1082   critical values associated with landslides in Povoação County (São Miguel Island,

1083   Azores): relationships with the North Atlantic Oscillation, *Hydrological Processes*,

1084   22(4), 478

1085   Masson, D. G., (1996), Catastrphic collapse of the volcanic island of Hierro 15 ka ago and

1086   the history of landslides in the Canary islands, *Geology*, 24 (3), 231-234

1087   Masson, D. G., A. B. Watts, M. J. R. Gee, R. Urgeles, N. C. Mitchell, T. P. Le Bas, and

1088   M. Canals (2002), Slope failures on the flanks of the western Canary Islands, *Earth*

1089   *Science Reviews, 57*, 1-35, PII: S0012-8252Ž01.00069-1

1090   Masson, D. G., C. B. Harbitz, R. B. Wynn, G. Pedersen and F. Lovholt (2006), Submarine

1091   landslides: processes, triggers and hazard prediction, *Philosophical Transactions of*

1092   *the Royal Society, 364*, 2009-2039, doi:10.1098/rsta.2006.1810

1093   Masson, D. G., T. P. Le Bas, I. Grevemeyer and W. Weinrebe (2008), Flank collapse and

1094   large‐scale landsliding in the Cape Verde Islands, off West Africa, *Geochemistry,*

1095   *Geophysics, Geosystems*, 9(7)

1096   McGuire, W. J, R. J. Howarth, C. R. Firth, A. R. Solow, A. D. Pullen, S. J. Saunders, I. S.

1097   Stewart, and C. Vita-Finzi (1997), Correlation between rate of sea-level change and

1098   frequency of explosive volcanism in the Mediterranean. *Nature,* 389, 473 - 477.

1099   McMurty, G. M., E. Herrero-Bervera, M. D. Cremer, J. R. Smith, J. Resig, C. Sherman

1100   and M. E. Torresan (1999), Stratigraphic constraints on the timing and emplacement

1101   of the Alika 2 giant Hawaiian submarine landslide, *Journal of Volcanology and*

1102   *Geothermal Research*, 94, 35-58

1103   McMurtry, G. M., P. Watts, G. J. Fryer, J. R. Smith and F. Imamura (2004a), Giant

1104   landslides, mega-tsunamis, and paleo-sea level in the Hawaiian Islands, *Marine*

1105   *Geology*, 203,219–233, doi:10.1016/S0025-3227(03)00306-2

1106 McMurtry, G. M., G. J. Fryer, D. R. Tappin, I. P. Wilkinson, M. Williams, J. Fietzke, D.

1107   Garbe-Schoenberg and P. Watts (2004b), Megatsunami deposits on Kohala volcano,

1108   Hawaii, from flank collapse of Mauna Loa, *Geology*, 32(9),741–744, doi:

1109   10.1130/G20642.1

1110 Miller, K. G., M. A. Kominz, J. V. Browning, J. D. Wright, G. S. Mountain, M. E. Katz,

1111   P. J. Sugarman, B. S. Cramer, N. Christie-Blick and S. F. Pekar (2005), The

1112   Phanerozoic Record of Global Sea-Level Change, *Science, 310*, 1293-1298, doi:

1113   10.1126/science.1116412

1114 Moore, J. G., D. A. Clague, R. T. Holcomb, P. W. Lipman, W. R. Normark, and M. E.

1115   Torresan (1989), Prodigious submarine landslides on the Hawaiian Ridge, *Journal of*

1116   *Geophysical Research: Solid Earth*, 94(B12), 17465-17484

1117 Moore, J. G., D. A. Clague, R. T. Holcomb, P. W. Lipman, W. R. Normark and M. E.

1118   Teorresan (1992), Prodigious submarine landslides on the Hawaiian Ridge, *Journal*

1119   *of Geophysical Research*, 94(89), 17465-17484

1120 Moore, J. G. and R. T. Holcomb (1994), Giant Hawaiian lantslides, *Earth and Planetary*

1121   *Science Letters*, 22, 119–144

1122 Moriya, I. (2003), Toya Caldera, *In Regional geomorphology of the Japanese islands,*

1123   Edited by T. Koaze, M. Nogami, Y. Ono, and K. Hirakawa, *University of Tokyo*

1124   *Press,* 2, 281–288

1125 Nakada, M. and H. Yokose (1992), Ice age as a trigger of active quaternary volcanism and

1126   tectonism, *Tectonophysics,* 212, 321-329

1127 Oehler, J. F. (2005), Les déstabilisations de flanc des volcans de l'Ile de La Réunion. Mise

1128   en évidence, implications et origines. PhD Thesis, Univ. Blaise Pascal, Clermont-

1129   Ferrand

1130 Oehler, J. F., J. F. Lénat and P. Labazuy (2008), Growth and collapse of the Reunion

1131   Island volcanoes, *Bulletin of Volcanology,* 70, 717–742, doi: 10.1007/s00445-007-

1132   0163-0

1133 Ogg, J. G. (2012), Geomagnetic Polarity Time Scale. *In: The Geologic Time Scale 2012*,

1134   Edited by F. M. Gradstein, J. G. Ogg, M. D. Schmitz and G. M. Ogg, *Elsevier*

1135   *Publishing*, 85-114

1136 Palmer, M. R., S. J. Hatter., T. M. Gernon., R. N. Taylor., M. Cassidy. et al (2016),

1137   Discovery of a large 2.4 Ma Plinian eruption of Basse-Terre, Guadeloupe, from the

1138   marine sediment record, *Geology, 44*(2), 123-126

1139 Paris, R., T. Giachetti., J. Chevalier., H. Guillou and N. Frank (2011), Tsunami deposits

1140   in Santiago Island (Cape Verde archipelago) as possible evidence of a massive flank

1141   failure of Fogos volcano, *Sedimentary Geology,* 239(3), 129-145

1142 Paterne, M. (1980), Chronologie des éruptions ré- centes du massif de la Soufrière

1143   (Guadeloupe— Petites Antilles). Essai de comparaison des périodes d'activité

1144   volcanique de quelques grandes régions volcaniques [3rd cycle thesis]: Bordeaux,

1145   France, Université de Bordeaux, no. 1606, 165 p.

1146 Pope. E. L., P. J. Talling, M. Urlaub, J. E. Hunt, M. A. Clare and P. Challenor, (2015),

1147   Are large submarine landslides temporally random or do uncertainties in available

1148   age constraints make it impossible to tell? *Marine Geology,* 369, 19-33

1149   Quidelleur, X., A. Hildenbrand and A. Samper (2008), Causal link between Quaternary

1150   paleoclimatic changes and volcanic islands evolution, *Geophysical Research Letters*,

1151   *35*, 1–5, doi:10.1029/2007GL031849

1152   Radiosonde data downloaded from http://www1.ncdc.noaa.gov/pub/data/igra/ from

1153   directory data-por/, Download file for Le Reuzet station in Guadeloupe, code GP,

1154   numeric code 78897

1155   Ramalho, R. S., G. Winckler, J. Madeira, G. R. Helffrich, A. Hipólito, R. Quartau and J.

1156   M. Schaefer (2015), Hazard potential of volcanic flank collapses raised by new

1157   megatsunami evidence, *Science advances*, 1(9), e1500456

1158   Reid, R.P., S. N. Carey and D. R. Ross (1996), Geological Society of America Bulletin

1159   Late Quaternary sedimentation in the Lesser Antilles island arc Late Quaternary

1160   sedimentation in the Lesser Antilles island arc, *Geological society of America*

1161   *Bulletin, 108*, 78-100, doi: 10.1130/0016-7606(1996)108<0078:LQSITL>2.3.CO;2

1162   Reid, M.E. (2004), Massive collapse of volcano edifices triggered by hydrothermal

1163   pressurization, *Geology,* 32, 373-376

1164   Samper, A., X. Quidelleur, P. Lahitte. D. Mollex (2007), Timing of effusive volcanism

1165   and collapse events within an oceanic arc island: Basse-Terre, Guadeloupe

1166   archipelago (Lesser Antilles Arc), *Earth and Planetary Science Letters, 258*, 175-

1167   191, doi:10.1016/j.epsl.2007.03.030

1168   Samper. A., Quidelleur. X., Boudon. G., Le Friant., A., Komorowski. J. C. (2008),

1169   Radiometric dating of three large volume flank collapses in the Lesser Antilles Arc,

1170   *Journal of Volcanology and Geothermal Research*, 176, 485-492

1171   Sato, H. P., H. Hasegawa., S. Fujiwara., M. Tobita., M. Koarai., H. Une and J. Iwahashi

1172   (2007), Interpretation of landslide distribution triggered by the 2005 Northern

1173   Pakistan earthquake using SPOT 5 imagery, *Landslides*, 4(2), 113-122

1174   Seta, M. D. et al., (2012), Slope instability induced by volcano-tectonics as an additional

1175   source of hazard in active volcanic areas: The case of Ischia island (Italy), *Bulletin of*

1176   *Volcanology*, 74, 79–106

1177   Siebert, L. (1984), Large volcanic debris avalanches: characteristics of source areas, de-

1178   posits, and associated eruptions, *Journal of Volcanology and Geothermal Research*,

1179   22, 163–197

1180   Singer, B. S., B. R. Jicha, M. A. Harper, J. A. Naranjo, L. E. Lara and H. Moreno-Roa,

1181   (2008), Eruptive history, geochronology, and magmatic evolution of the Puyehue-

1182   Cordón Caulle volcanic complex, Chile, *Geological Society of America Bulletin, 120*

1183   *(5/6)*, 599-618, doi: 10.1130/B26276.1

1184   Soya, T., Y. Katsui, K. Niida, K. Sakai and A. Tomiya (2007), Geologic map of Usu

1185   volcano, 2nd edition, Geological Map of Volcanoes (2), Geological Survey of Japan,

1186   The National Institute of Advanced Industrial Science and Technology, Tsukuba

1187   Stillman, C. J. (1999), Giant Miocene landslides and the evolution of Fuerteventura,

1188   Canary Islands, *Journal of Volcanological and Geothermal Research,* 94(1-4), 89–

1189   104.

1190   Trofimovs, J. et al., (2006), Submarine pyroclastic deposits formed at the Soufrière Hills

1191   volcano, Montserrat (1995–2003): What happens when pyroclastic flows enter the

1192   ocean? *Geology*, *34(7)*, 549-552, doi: 10.1130/G22424.1

1193   Trofimovs, J., R. S. J. Sparks and P. J. Talling (2008), Anatomy of a submarine

1194   pyroclastic flow and associated turbidity current: July 2003 dome collapse, Soufrière

1195   Hills volcano, Montserrat, West Indies, *Sedimentology*, *55*, 617-634, doi:

1196   10.1111/j.1365-3091.2007.00914

1197   Trofimovs, J., J. K. Fisher, H. A. MacDonald, P. J. Talling, R. S. J. Sparks, M. B. Hart, C.

1198   W. Smart, G. Boudon, C. Deplus, J. C. Komorowski, A. Le Friant, S. G. Moreton,

1199   S.G and M. J. Leg (2010), Evidence for carbonate platform failure during rapid sea-

1200   level rise; ca 14 000 year old bioclastic flow deposits in the Lesser Antilles.

1201   *Sedimentology*, *57*, 735-759, doi: 10.1111/j.1365-3091.2009.01117

1202   Trofimovs, J., C. Foster, R. S. J. Sparks, S. Loughlin, A. Le Friant, C. Deplus, L. Porritt,

1203   T. Christopher, R. Luckett, P. J. Talling, M. R. Palmer and T. Le Bas (2012),

1204   Submarine pyroclastic deposits formed during the 20th May 2006 dome collapse of

1205   Soufrière Hills volcano, Montserrat, *Bulletin of Volcanology, 74*, 391-405, doi:

1206   10.1007/s00445-011-0533-5

1207   Trofimovs, J., P. J. Talling, J. K. Fisher, M. B. Hart, R. S. J. Sparks, S. F. L. Watt, M.

1208   Cassidy, C. W. Smart, A. Le Friant, S. G. Moreton and M. J. Lang (2013), Timing,

1209   origin and emplacement dynamics of mass flows offshore of SE Montserrat in the

1210   last 110 ka: Implications for landslide and tsunami hazards, eruption history, and

1211   volcanic island evolution, *Geochemistry, Geophysics, Geosystems*, *14(2)*, 385–406.

1212   doi:10.1002/ggge.20052

1213   Urgeles, R., M. Canals, J. Baraza and B. Alonso (1997), The most recent megalandslides

1214   of the Canary Islands: El Golfo debris avalanche and Canary debris flow, west El

1215   Hierro Island, *Journal of Geophysical Resarch*, 102, 20305-20323

1216 Urgeles, R., D. G. Masson, M. Canals, A. B. Watts and T. Le Bas (1999), Recurrent

1217   large-scale landsliding of the west flank of La Palma, Canary Islands, *Journal of*

1218   *Geophysical Research*, 104 (B11), 25331-25348, doi: 1999JB900243 0148-

1219   0227/99/1999JB 900243$09.00

1220 Vezzoli, L., (1988), Island of Ischia, *CNR Quaderni de La ricerca scientifica*, 114(10),

1221   122

1222 Vincent, P. M., J. L. Bourdier, G. Boudon (1989), The primitive volcano of Mount Pelée:

1223   its construction and partial destruction by flank collapse, *Journal of volcanology and*

1224   *geothermal research*, 38(1), 1-15

1225 Wadge, G. (1985), Morne Patates volcano, Southern Dominica, Lesser Antilles,

1226   *Geological Magazine*, *122 (3)*, 253–260

1227 Wadge. G., B. Voight, R. S. J. Sparks, P. D. Cole, S. C. Loughlin, and R. E. A. Robertson

1228   (2014), An overview of the eruption of Soufrière Hills Volcano, Montserrat from

1229   2000 to 2010, *in The Eruption of the Soufrière Hills Volcano, Montserrat from*

1230   *2000–2010, Memoirs of the Geological Society of London 3*, edited by G. Wadge, R.

1231   A. E.Robertson, and B. Voight, *Geological Society of London,*1–4

1232 Wall-Palmer, D., et al., (2014), Late Pleistocene stratigraphy of IODP Site U1396 and

1233   compiled chronology offshore of south and south west Montserrat, Lesser Antilles,

1234   *Geochemistry, Geophysics, Geosystems*, *15*, 1–21, doi: 10.1002/2014GC005402/full

1235 Ward, S. N. and S. Day (2003), Ritter Island Volcano-lateral collapse and the tsunami of

1236   1888, *Geophysical Journal International, 154*, 891-902

1237   Watt, S. F. L., et al., (2012a), Combinations of volcanic-flank and seafloor-sediment

1238   failure offshore Montserrat, and their implications for tsunami generation, *Earth and*

1239   *Planetary Science Letters*, *319(320)*, 228–240, doi:10.1016/j.epsl.2011.11.032

1240   Watt, S. F. L., et al., (2012b), Widespread and progressive seafloor-sediment failure

1241   following volcanic debris avalanche emplacement: Landslide dynamics and timing

1242   offshore Montserrat, Lesser Antilles, *Marine Geology*, *323(325)*, 69–94,

1243   http://dx.doi.org/10.1016/j.margeo.2012.08.002

1244   Watt, S. F. L., P. J. Talling and J. E. Hunt (2014), New insights into the emplacement

1245   dynamics of volcanic island landslides, *Oceanography,* 27, 46–57

1246   Weaver, P. P. E., R. G. Rothwell, J. Ebbing, D, Gunn and P. M. Hunter (1992),

1247   Correlation, frequency of emplacement and source directions of megaturbidites on

1248   the Madeira Abyssal Plain, *Marine Geology*, 109(1-2), 1-20

1249

1250

1251   Figure 1. Topographic and bathymetric map of Montserrat showing site of U1395B and

1252   large debris avalanche flows [Le Friant et al., 2004; Boudon et al., 2007; Lebas et al.,

1253   2011; Watt et al., 2012a, 2012b] .

1254

1255   Figure 2: Upper 44 m of Hole U1395B including core log and photos; calculated

1256   sedimentation rates for all age models; NRM declination data from shipboard

1257   measurements; section of stratigraphic core photos and log; sample of componentry data;

1258   oxygen isotopes from this study and the global oxygen isotope curve from Lisiecki and

1259   Raymo [2005]. For full componentry data and stratigraphic log of Hole U1395B see

1260   supplementary data.

1261

1262   Figure 3: Correlations of the top of core U1395B with shallow cores based on

1263   componentry and oxygen isotope data [Le Friant et al., 2008; Cassidy et al., 2012b, 2013;

1264   Ogg et al., 2012; Trofimovs et al., 2013; Wall-Palmer et al., 2014].

1265

1266   Figure 4: Timing of (a) all events, (b) volcaniclastic events (tephra fall and turbidite

1267   deposits; including mixed composition turbidites), (c) volcaniclastic events (tephra fall

1268   and volcaniclastic turbidite), (d) tephra fall deposits, and (e) all turbidites at Montserrat.

1269   In each case, three different age models are shown. Age model 1 (green) uses oxygen

1270   isotope data, biostratigraphic data, AMS dates, and paleomagnetic dates. Age model 2

1271   (red) uses Deposit 2 as a boundary at 130 ka (Figure 2), and the paleomagnetic intervals.

1272   Age model 3 (blue) uses only the paleomagnetic data. Clustering of events in all age

1273   models can be seen at ~950-860 ka, 810-750 ka, 200-100 ka and from ~50 ka, on

1274   Montserrat. There is an absence of prolonged pauses in activity. Thin grey lines show

1275   occurrence of scoria within core U1395B, the thick grey line shows known extents of

1276   activity at volcanic centres on Montserrat based on limited subaerial dating [Harford et al.,

1277   2002].

1278

1279   Figure 5: Number of events within 50 kyr (centred on window, at 10 kyr increments).

1280   Peaks correspond to clusters in Figure 4. Age model 1 (green) uses oxygen isotope data,

1281   biostratigraphic data, AMS dates, and paleomagnetic dates. Age model 2 (red) uses

1282   Deposit 2 as a boundary at 130 ka (Figure 2), and the paleomagnetic intervals. Age model

1283   3 (blue) uses only the paleomagnetic data. Peaks in event frequency occur at ~930 ka to

1284   ~900 ka, ~810 ka to ~760 ka, and ~190 ka to ~120 ka. Periods when event frequency is

1285   above the 90% confidence interval in all age models are shaded in grey. The black line is

1286   the Miller et al., [2005] sea-level curve in meters from present day sea-level. Thin grey

1287   lines show occurrence of mafic scoria within Hole U1395B, the thick grey line shows

1288   known extents of activity at volcanic centres on Montserrat based on limited subaerial

1289   dating [Harford et al., 2002]. There is a peak in event frequency that coincides with the

1290   appearance of mafic scoria in Hole U1395B and all large flank collapses occur during

1291   periods of rapid sea-level rise.

1292

1293   Figure 6: A. Diagram summarising the age of large (>0.3 km^3) landslides around

1294   volcanic islands and sea-level. The sea-level curve used is Miller et al., [2005]. Events

1295   considered have date errors of <±22.5 ka. Periods of rapid sea-level rise (>5m/ka)

1296   are highlighted in blue. Vertical bars show errors of individual landslide ages. Ocean

1297   island landslides are shown in green, and island arc landslides are shown in red.

1298   Letters identify indiviual landslides and correspond to letters in Table 3. B.

1299   Comparison of sea level conditions with those at the time of documented landslides

1300   (Table 3) using data in 5 ka bins. Grey solid circles indicate the full range of conditions

1301   over the past 1 Ma at which no landslides were recorded. Annotated box and whisker

1302   plots indicate the spread of each data set, with boxes showing 25%, 50% and 75% of the

1303   data, whiskers showing the minimum and maximum. Numbers next to data points show

1304   the number of overlapping datum. A general skew of landslides occurring at rapid sea-

1305   level rises can be seen in the box and whisker plots.

1306

1307

1308

1309

Allocation number	Publication code	Sample identifier	$\delta^{13}C_{VPDB}$‰ ± 0.1	Carbon content (% by wt.)	^{14}C Enrichment (% modern)	+/- 1σ (% modern)	Conventional Radiocarbon Age (years BP)	+/- 1σ (radiocarbon yrs BP)	Stratigraphic position (cm)
1721.0513	SUERC-46961	1H2W-108-110	1.1	10.9	28.82	0.13	9993	37	258-260
1721.0513	SUERC-46962	1H2W-115-117	1.1	10.8	23.93	0.12	11489	40	265-267
1721.0513	SUERC-46965	1H3W-109-111	1.2	11.4	0.33	0.06	45806	1463	409-411
1721.0513	SUERC-46966	1H3W-116-118	1.0	11.3	0.40	0.06	44294	1208	416-418

1310 Table 1: AMS carbon dates from core U1395.

1311

	Age Model 1	**Age Model 2**	**Age Model 3**
Linear model	0.0898	*0.00176*	*0.00285*
Generalised linear model	0.083407	*0.00138*	*0.00696*
Proportional hazards model	0.106	*0.00219*	*0.00942*

1312 Table 2: Results of linear statistical tests for turbidite frequency and sea-level correlations. Italicised values show when statistical tests are

1313 significant, (ie when the null hypothesis can be rejected).

1314

1315   Table 3: Global landslide database for ocean island landslides and island arc landslides

1316   with volumes >0.3 km^3 and with age errors of < ±22.5 kyr.

1317

1318

1319

1320

1321

1322

1323

1324

1325

1326
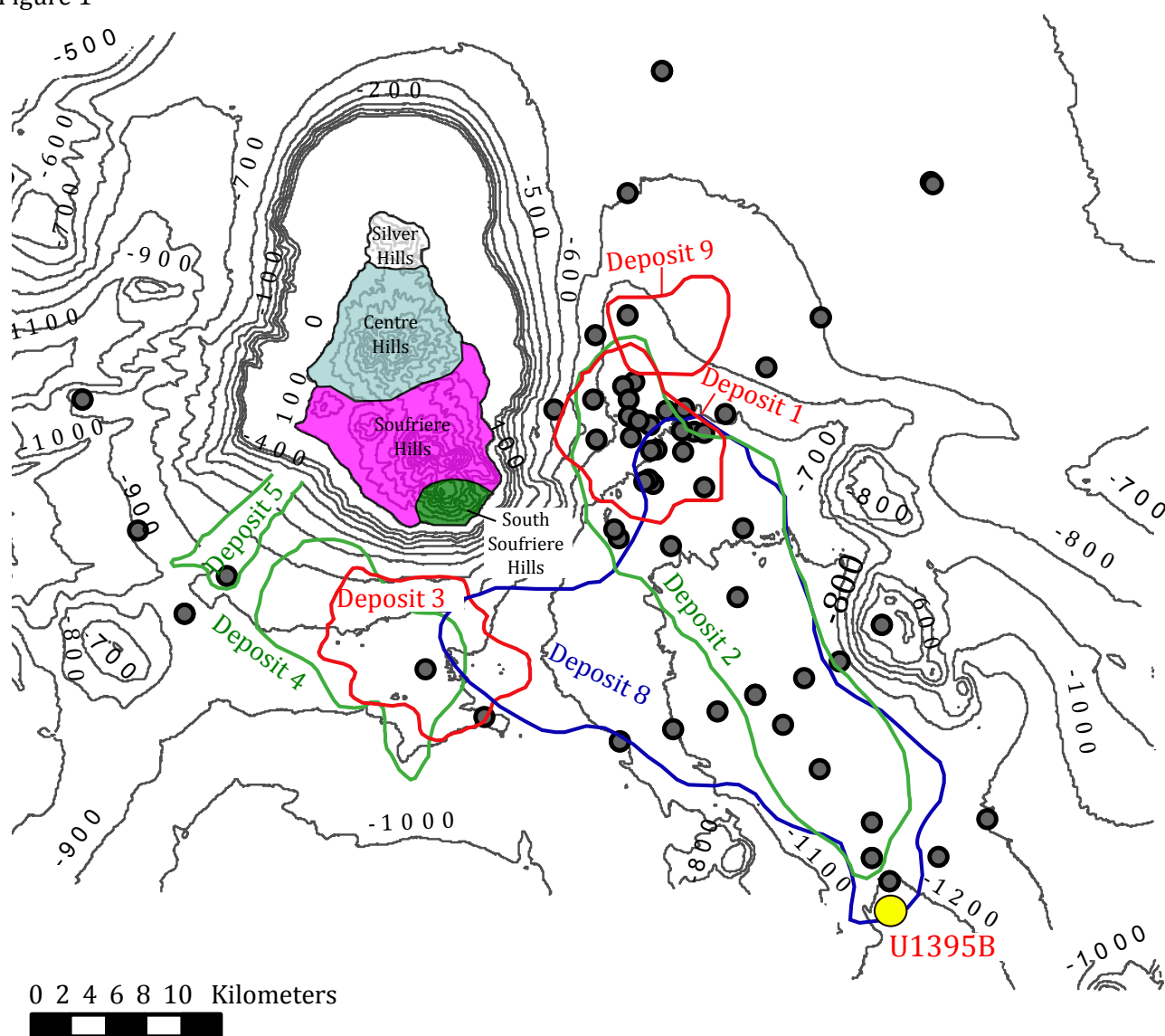
1327

1328

1329

1330

1331

1332

1333

1334

1335

1336

1337

1338

1339

Flank collapse name	Country/ Island	Age (ka)	Volume (km³)	References	Letter in Supplement -ary Figure S4
Ocean Islands					
El Golfo	Canary Islands, El Heirro	20-10	150	Weaver et al., [1992]; Longpre et al., [2011]; Hunt et al., [2013]	a
El Julan	Canary Islands, El Heirro	550-530	130	Hunt et al., [2013]	b
Cumbre Nueva	Canary Islands, La Palma	574-529	95	Costa et al. [2014]	c
Icod	Canary Islands, Tenerife	170-160	320	Ancochea et al., [1990]; Wynn et al., [2002]; Carraceado et al., [2007]; Hunt et al., [2013, 2014]	d
Orotava	Canary Islands, Tenerife	566-525	1000	Watts and Masson [1995]; Masson et al., [2002]; Boulestreix et al., [2013]; Hunt et al., [2013]	e
Guimar	Canary Islands, Tenerife	860-840	120	Krastel et al., [2001]	f
Fogo	Cape Verde	80-66	160	Ramalho et al., [2015]	g
Alika 2	Hawaii, Mauna Loa	132-122	>0.5	McMurty et al. [1999]	h
Tahiti North	Tahitian Archipelago, Tahiti	870-850	800	Clouard et al., [2000]; Hildenbrand et al., [2004, 2006].	i
Island Arcs					
Carmichaël	Lesser Antilles, Guadeloupe	11.5-6.9	0.3	Boudo et al., [1984, 2007]	j
Carbet	Lesser Antilles, Guadeloupe	3.5-2.8	0.5	Boudon et al., [1984, 2007]; Jerime [1979]; Paterne [1980]; Daigun [1981]; Daigun et al., [1981]	k
La Soufriere	Lesser Antilles, Dominica	6.7-2.3	6 to 7	Le Friant et al., [2002]; Boudon et al., [2007]	l
South	Italy, Ischia	3-2.4	1.5	de Alteriis et al., [2010, 2014]	m
Piettre Rosse	Italy, Ischia	40-2.4	>0.3	Vezzoli [1988]; Buchner [1986]; Seta et al., [2012]	n
Falanga	Italy, Ischia	2.4	>0.3	Buchner [1986]; Seta et al., [2012]	o
Casamicciola (NDDe)	Italy, Ischia	2.8	>0.3	de Vita et al., [2010]; Seta et al., [2012]	p
NDDw	Italy, Ischia	<10 ka		Vezzoli et al., [1988]; de Aleriis and Violante, [2009]; Seta et al., [2012]	q
D1	Lesser Antilles Martinique	129-124	>25	Germa et al., [2011]	r
D2 or the St Pierre event	Lesser Antiiles, Martinique	23.6-26.4	13	Vincent et al., [1989]; Le Friant et al., [2003]	s
D3 or Rivière Sèche event	Lesser Antiiles, Martinique	9.8-8	2	Le Friant et al., [2003]; Boudon et al., [2007]	t
Usu	Japan, Hokkaido	8-7	1 to 2	Moriya, [2003] (in Japanese); Soya et al., [2007]; Yoshida et al., [2012]	u
Ritter	Papua New Guinea, Ritter Island	0.1	5	Cooke [1981]; Ward and Day [2003]	v
Deposit 1	Lesser Antilles, Montserrat	14-11	1.8	Trofimovs et al. [2013]; Watt et al. [2012a], [2012b]; Le Friant et al. [2004]; Lebas et al. [2011]	w
Deposit 2	Lesser Antilles, Montserrat	146-112	9	Harford et al. [2002]; Le Friant et al. [2004]; Lebas et al. [2011]; Watt et al. [2012a], [2012b]; Crutchley et al. [2013]	x
Deposit 5	Lesser Antilles, Montserrat	12-8	0.3	Cassidy et al. [2013]; Le Friant et al. [2004]; Lebas et al. [2011]	y

Figure 1

Figure 2

Figure 3

CAR-MON 2   JR123-6V   JR123-5V   U1394B   U1395B   U1396C   Global (Lisiecki and Raymo 2005)

KEY

- hemipelagic mud
- bioclastic turbidite
- mixed turbidite
- volcaniclastic turbidite
- tephra fall
- 6186 radiocarbon ages from Trofimovs et al., (2013) and Coussens et al., (2016)

F.O. E Huxleyi

Figure 4

Figure 5

Figure 6